

Expectations for the muon $g - 2$ in simplified models with dark matter

Kamila Kowalska^{1,a} and Enrico Maria Sessolo,^{1,2,b}

¹ *Institut für Physik, Technische Universität Dortmund,
D-44221 Dortmund, Germany*

² *National Centre for Nuclear Research,
Hoża 69, 00-681 Warsaw, Poland*

Abstract

We investigate simplified models of new physics that can accommodate the measured value of the anomalous magnetic moment of the muon and the relic density of dark matter. We define a set of renormalizable, $SU(2) \times U(1)$ invariant extensions of the Standard Model, each comprising an inert \mathbb{Z}_2 -odd scalar field and one or more vector-like pairs of colorless fermions that communicate to the muons through Yukawa-type interactions. The new sectors are classified according to their transformation properties under the Standard Model gauge group and all models are systematically confronted with a variety of experimental constraints: LEP mass bounds, direct LHC searches, electroweak precision observables, and direct searches for dark matter. We show that scenarios featuring only one type of new fermions become very predictive once the relic density and collider constraints are taken into account, as they do not introduce explicit sources of chiral-symmetry violation. Conversely, for models where this violation is generated via fermion mixing, the constraints are much looser and new precision experiments with highly suppressed systematic uncertainties are required to test the parameter space.

^{*a} `kamila.kowalska@tu-dortmund.de`

^{†b} `enrico.sessolo@ncbj.gov.pl`

Contents

1	Introduction	2
2	Muon $g - 2$ contributions from scalar interactions	4
3	Muophilic portal models	6
3.1	Models with a real neutral scalar singlet	7
3.2	Models with a complex neutral scalar singlet	10
3.3	Models with a scalar doublet	11
4	Experimental constraints	14
4.1	Electroweak precision observables	14
4.2	Collider constraints	17
5	Numerical analysis	18
5.1	Real scalar with a singlet or doublet VL fermion	19
5.2	Real scalar with mixing singlet and doublet VL fermions	22
5.3	Complex singlet scalar with VL fermions	23
5.4	Doublet scalar with singlet, doublet, or triplet VL fermions	25
6	Summary and conclusions	29

1 Introduction

When the anomalous magnetic moment of the muon, $(g - 2)_\mu$, was measured at BNL several years ago [1], it showed a discrepancy with the Standard Model (SM) expectation that has since been widely interpreted as a hint for new physics not far from the electroweak symmetry-breaking (EWSB) scale. After taking into account a recent update [2] of the lowest-order hadronic contributions to the SM calculation, the discrepancy, $\delta(g - 2)_\mu$, is estimated to be at the level of $\sim 3.5\sigma$: $\delta(g - 2)_\mu = (27.4 \pm 7.6) \times 10^{-10}$. (A second recent review of the hadronic vacuum polarization contributions and uncertainties [3] yields an even more convincing $\delta(g - 2)_\mu = (31.3 \pm 7.7) \times 10^{-10}$.)

While the interest in this anomaly never really went away, it is bound to receive a boost by the start of the new Muon $g-2$ experiment at Fermilab [4,5], which will improve the statistical precision of the measurement by a factor of four or so with respect to BNL. Additionally, just a few years after the Fermilab experiment, $(g - 2)_\mu$ will also be measured at J-PARC [6–10], which is expected to reach a comparable sensitivity even if the experimental setup is different.

From the theory standpoint, the anomaly can be accommodated in many scenarios beyond the Standard Model (BSM) (see, e.g., [11] for a comprehensive review). Early on, the impact of new physics 1-loop contributions to $\delta(g - 2)_\mu$ [12, 13] was investigated predominantly in the framework of supersymmetry [14–24], but the consequences of a positive measurement for more generic models were also explored [25, 26]. Recently, among the large number of studies appearing every year on the topic, Ref. [27] and Refs. [28, 29] have adopted a systematic approach based on simplified models instead of focusing on specific

constructions. Simplified models are characterized by a limited number of free parameters and classified according to the gauge quantum numbers of the particles introduced and the Lorentz structure of their interactions, and can be confronted with a variety of experimental information, like LEP/LHC constraints in [27] or flavor observables in [29].

In this paper, extending the approach of [27–29], we try to answer the following question: in case a positive measurement of $\delta(g-2)_\mu$ is obtained with large significance at Fermilab, what information can we infer on the couplings, masses, and quantum numbers of the new particles involved in the process, provided we require that the same physics also yields the relic density of dark matter in the Universe. As the nature of dark matter constitutes one of the greatest mysteries in contemporary particle physics, we think it is enticing to entertain the idea that a positive measurement at Fermilab and J-PARC could open a window into the nature of the dark sector, possibly in conjunction with other experimental signatures. In fact, we will show that requiring the same physics to be responsible for the $(g-2)_\mu$ anomaly and dark matter leads to strong bounds on the allowed parameter space and introduces a series of complementary signatures, in particular at the high-luminosity LHC, in future electroweak precision experiments and, to a lesser extent, in dark matter direct detection searches.

Obviously, this complementary approach is not original. It is invoked for instance in supersymmetry, where neutralinos, sleptons, and charginos often provide at the same time a good fit to $\delta(g-2)_\mu$ and the correct relic abundance. It has also been recently adopted for other BSM models [30], and there exists at least one previous study of possible complementary signatures for $(g-2)_\mu$ and dark matter in simplified models based on a minimal set of assumptions [31].

Like Ref. [31], we define a set of minimal extensions of the SM that provide a viable weakly interactive massive particle (WIMP) dark matter candidate and have the potential to give a positive signal in the upcoming $(g-2)_\mu$ experiments. Unlike that work, however, we will not employ the effective field theory approach, nor limit ourselves to SM singlets in the interactions with the muons. Rather, inspired by of Ref. [27], we consider a set of scenarios in which both the dark matter and the BSM lepton mediator can transform non-trivially under the SU(2) gauge group. We will also always adopt the relic abundance as an important constraint on the parameter space.

The models we construct are based on the following requirements:

- The dark matter interacts with the muons through renormalizable couplings
- Interactions are CP conserving and invariant under the SM gauge group, $SU(2) \times U(1)$
- Each model satisfies the constraints from perturbativity and unitarity
- The measurement of the relic abundance is an active constraint on the parameter space.

We do not consider in this paper dark matter lighter than the mass of the muon so that, to make it stable, we introduce as usual an additional discrete symmetry, \mathbb{Z}_2 , under which the dark matter is odd and the SM is even. Also note that the dark matter must be *leptophilic* to evade the stringent current bounds from direct detection experiments, and for this reason we neglect dark-matter interactions with quarks.

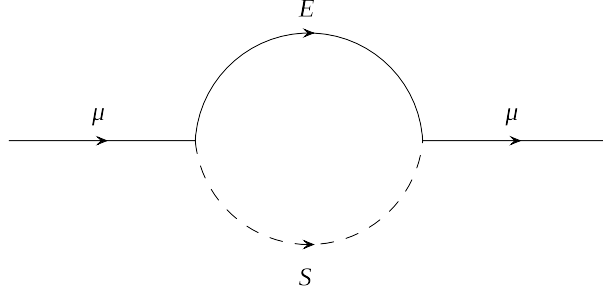


Figure 1: The 1-loop contribution to $\delta(g - 2)_\mu$ in the presence of a new scalar field S and a new lepton E . A photon line attached to whichever particle is electrically charged is implied.

The first of the requirements listed above limits the allowed interactions to fermion–(pseudo)scalar–fermion and fermion–(axial)vector–fermion types. As one of the participating fermions is necessarily the muon, the discrete symmetry forces us to additionally introduce \mathbb{Z}_2 -odd colorless fermions, which must be *vector-like* (VL) to evade the bounds from electroweak precision observables (EWPOs) and to not introduce gauge anomalies.

Note that all our assumptions are trivially satisfied by Yukawa-type interactions fermion–(pseudo)scalar–fermion, once the appropriate scalar potential is spelled out. Conversely, interactions involving (axial)vector particles require additional assumptions, namely the definition of extra dark gauge groups and charges, as well as a careful treatment of lepton-flavor violating processes. For this reason, in this paper we limit ourselves to discussing fermion–(pseudo)scalar–fermion interactions only.

For the sake of simplicity, and unlike Refs. [27,31], we also do not require universal Yukawa interactions of the BSM sector with the SM leptons, which could give extra constraints from LEP measurements. We rather assume that the new scalars and fermions couple exclusively the SM muons. Lepton-flavor violating processes are obviously absent in such a setup. This assumption may seem somewhat *ad hoc*, but it allows us to focus on effects arising in the muon sector only, without imposing additional model-dependent symmetries aimed at enforcing Minimal Flavor Violation. It can also perhaps be seen as realistic in light of the recent flavor anomalies at LHCb [32], which seem to point to the existence of lepton-flavor non-universality.

The paper is organized as follows. In Sec. 2 we briefly review the expressions of the 1-loop new physics contributions to $(g - 2)_\mu$ in the case of scalar couplings. In Sec. 3 we introduce the Lagrangians of our simplified models and describe their couplings to the muons. In Sec. 4 we review the constraints we apply, and in Sec. 5 we present and extensively discuss the results of our numerical analyses. We finally summarize our findings and conclude in Sec. 6.

2 Muon $g - 2$ contributions from scalar interactions

The generic 1-loop contribution to the muon anomalous magnetic moment involving the \mathbb{Z}_2 -odd sector is schematically shown in Fig. 1, where at least one of the particles in the loop must be electrically charged, and there is an implied photon line attached to the charged

propagator. The most generic Yukawa interaction pictured in the vertices of Fig. 1 reads

$$\mathcal{L} = g_s \bar{\psi}_E \psi_\mu \phi_S + i g_p \bar{\psi}_E \gamma^5 \psi_\mu \phi_S + \text{h.c.} \quad (1)$$

in terms of a scalar coupling g_s (or a pseudoscalar coupling g_p) of the muon to a generic heavy fermion, E , and a scalar, S .

The specific value of $(g - 2)_\mu$ depends on the electric charge and spin quantum numbers of the particles running in the loop. Considering, for example, a charged fermion and a neutral scalar, one gets (see, e.g., [11, 29] for a review of the calculation)

$$\delta(g - 2)_\mu = \frac{m_\mu^2}{8\pi^2 m_S^2} \left[(|g_s|^2 + |g_p|^2) \int_0^1 dx \frac{x^2(1-x)}{(1-x)(1-\lambda^2 x) + \epsilon^2 \lambda^2 x} + \epsilon (|g_s|^2 - |g_p|^2) \int_0^1 dx \frac{x^2}{(1-x)(1-\lambda^2 x) + \epsilon^2 \lambda^2 x} \right], \quad (2)$$

in terms of the mass ratios of the new particles to the muon, $\epsilon = m_E/m_\mu$, $\lambda = m_\mu/m_S$.

Note that the chiral structure of the underlying model plays a crucial role in determining the size of $(g - 2)_\mu$. If one sets $g_p = 0$, the dominant contribution in Eq. (2) arises from the second term, which is enhanced by a large factor ϵ . On the other hand, the presence of a non-zero pseudoscalar coupling will reduce the size of this term, and in the case when $|g_s| = |g_p|$ the only remaining contribution is the one in the first line of Eq. (2).

This well-known fact is often used to obtain, by simple inspection of the Lagrangian, back-of-the-envelope estimates of how well a specific model can perform with respect to $(g - 2)_\mu$. The prescription is best recast in terms of c_L and c_R , the couplings of the new physics to the left- and right-chiral Weyl components of the muon. One can explicitly write the scalar and pseudoscalar coupling of Eq. (1) as $g_s = (c_R + c_L)/2$ and $i g_p = (c_R - c_L)/2$, and the integrals can be easily calculated for $\epsilon\lambda$ fixed in the approximation $\lambda \ll 1$. By defining $\epsilon^2 \lambda^2 = m_E^2/m_S^2 \equiv r$, one gets

$$\int_0^1 dx \frac{x^2(1-x)}{1-x+rx} = \frac{2+3r-6r^2+r^3+6r \ln r}{6(r-1)^4} \equiv \mathcal{F}_1(r) \quad (3)$$

$$\int_0^1 dx \frac{x^2}{1-x+rx} = \frac{3-4r+r^2+2 \ln r}{2(r-1)^3} \equiv \mathcal{F}_2(r), \quad (4)$$

which lead to the well known formula

$$\delta(g - 2)_\mu = \frac{1}{16\pi^2} \sum_{S^0, E^\pm} \left[\frac{m_\mu^2}{m_S^2} (|c_L|^2 + |c_R|^2) \mathcal{F}_1(r) + 2 \frac{m_\mu m_E}{m_S^2} \Re(c_L c_R^*) \mathcal{F}_2(r) \right], \quad (5)$$

where we have generalized Eq. (2) to include all possible charged fermion and neutral scalar states coupling to the muon.

Equation (5) expresses the fact that much larger values of $(g - 2)_\mu$ can be expected if the new physics cross-couples to *both* chiral states of the muon, providing a chirality-flip term that is enhanced proportionally to the mass of the new fermions. Note, incidentally, that if $\Re(c_L c_R^*)$ is positive, $\delta(g - 2)_\mu$ is positive.

One can follow a similar procedure to derive the $(g-2)_\mu$ formula for the case of charged scalars and neutral fermions in the loop, obtaining

$$\delta(g-2)_\mu = \frac{1}{16\pi^2} \sum_{S^\pm, E^0} \left[-\frac{m_\mu^2}{m_S^2} (|c_L|^2 + |c_R|^2) \mathcal{G}_1(r) + 2 \frac{m_\mu m_E}{m_S^2} \Re(c_L c_R^*) \mathcal{G}_2(r) \right], \quad (6)$$

where

$$\mathcal{G}_1(r) \equiv \frac{1 - 6r + 3r^2 + 2r^3 - 6r^2 \ln r}{6(r-1)^4} \quad (7)$$

$$\mathcal{G}_2(r) \equiv \frac{-1 + r^2 - 2r \ln r}{(r-1)^3}. \quad (8)$$

This contribution is negative when either c_L or c_R are equal zero, but can become positive for $\Re(c_L c_R^*) \neq 0$.

Finally we will also need the contribution to $(g-2)_\mu$ from a doubly charged fermion and a charged scalar in the loop. In this work we will just use the one for the c_L coupling, which reads [27]

$$\delta(g-2)_\mu = \frac{1}{16\pi^2} \sum_{S^\mp, E^{\pm\pm}} \left(\frac{m_\mu^2}{m_S^2} |c_L|^2 \mathcal{H}_1(r) \right), \quad (9)$$

where $\mathcal{H}_1(r) = 2\mathcal{F}_1(r) + \mathcal{G}_1(r)$.

3 Muophilic portal models

Before we introduce our simplified models for $(g-2)_\mu$ and dark matter, we start by defining the notation we adopt throughout the paper.

We indicate the SM fields with lower-case letters and the new \mathbb{Z}_2 -odd fields with capital letters. The quantum numbers of the leptons and Higgs boson of the SM are

$$l : (\mathbf{1}, \mathbf{2}, -1/2) \quad e_R : (\mathbf{1}, \mathbf{1}, -1) \quad \phi : (\mathbf{1}, \mathbf{2}, 1/2), \quad (10)$$

with respect to $SU(3) \times SU(2) \times U(1)$. When written explicitly, the lepton doublet reads $l = (\nu_L, e_L)^T$ and the Higgs field is $\phi = [0, (v+h)/\sqrt{2}]^T$ after EWSB. The Dirac fermion of charge -1 is constructed as $\psi_e = (e_L, e_R)^T$, as usual.

For the SM muon Yukawa coupling we use the convention, in Weyl notation,

$$\mathcal{L} \supset -y_\mu \phi^c l e_R^* + \text{h.c.}, \quad (11)$$

with $\phi^c \equiv -i\sigma_2 \phi^*$.

As was discussed in Sec. 1, we limit ourselves to considering CP conserving, renormalizable Yukawa interactions. We extend the SM particle content with new heavy scalar fields and VL leptons, which provide generally safe extensions of the SM because they do not introduce gauge anomalies and they avoid the stringent bounds on chiral fermions from LEP and SLC precision measurements. In the context of non-supersymmetric models, VL leptons for the $(g-2)_\mu$ anomaly have also been considered in [25, 27, 30, 33–35].

We will next classify our models according to the transformation properties of the new scalar and fermion fields under the SM gauge group.

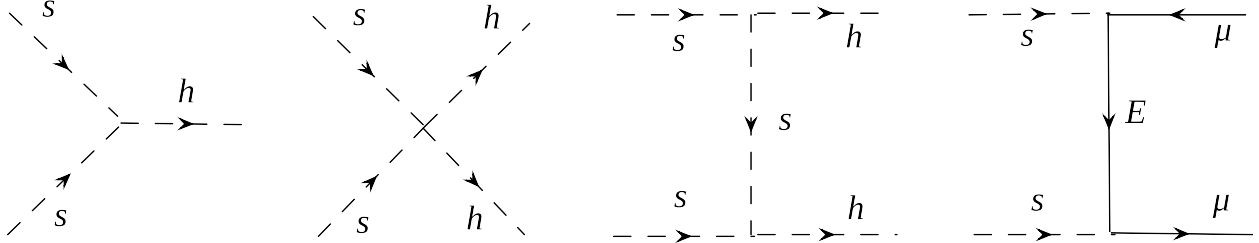


Figure 2: Starting from the left, the first 3 diagrams show the well-known scalar portal interactions that can potentially lead to the correct dark matter relic abundance. The last diagram on the right depicts the t -channel “bulk” mechanism via a new heavy fermion E .

3.1 Models with a real neutral scalar singlet

We begin with the simplest case, extending the SM by a singlet real scalar field,

$$s : (\mathbf{1}, \mathbf{1}, 0). \quad (12)$$

For simplicity, we assume in this work that any new introduced scalar is *inert*, in the sense that it does not develop a vacuum expectation value (vev).

The most general \mathbb{Z}_2 -symmetric renormalizable scalar potential that includes mass terms and quartic interactions for both the Higgs and the BSM scalar, as well as a portal coupling between the two, takes the form

$$V = -\mu^2 \phi^\dagger \phi + \frac{\lambda}{2} (\phi^\dagger \phi)^2 + \frac{\mu_s^2}{2} s^2 + \frac{\lambda_s}{2} s^4 + \lambda_{12} s^2 \phi^\dagger \phi, \quad (13)$$

in terms of 5 free parameters: μ and λ , the SM mass and quartic coupling, μ_s , λ_s , and the portal coupling λ_{12} . The tree level mass of the BSM scalar is in this case given by

$$m_s^2 = \mu_s^2 + \lambda_{12} v^2. \quad (14)$$

The parameters of the scalar potential are constrained by theoretical requirements. In order to guarantee that the electroweak vacuum is a global minimum, it is required that $\mu_s^2 + 2\lambda_{12} v_h^2 > 0$, where $v_h = v/\sqrt{2}$ is the vev of the neutral component of the Higgs scalar ϕ , and $v = 246$ GeV. One also needs $\mu_s^2 > 0$, so that the direction $v_h = 0, v_s \neq 0$ is not a minimum and the scalar s remains inert. The latter also guarantees that the \mathbb{Z}_2 symmetry is preserved in the electroweak broken phase. As a result, there is no mixing between the new scalar and the SM Higgs. Vacuum stability, i.e. requiring that the potential is bounded from below, requires $\lambda > 0$, $\lambda_s > 0$, and $\lambda_{12} > -\sqrt{\lambda\lambda_s}$. Moreover, perturbative unitarity bounds give $\lambda < 4.2$, $\lambda_s < 4.2$, and $\lambda_{12} < 25$.

The scalar potential given in Eq. (13) features well known dark matter properties (see [36–41] for early papers exploring the Higgs portal). The WIMP is here the scalar s , which efficiently annihilates in the early Universe through the interaction vertices depicted in the first three diagrams of Fig. 2. However, it is also well known that the portal coupling and dark matter mass are subject to strong bounds from direct detection searches, which, after the most recent bound from XENON-1T [42] are considered, exclude the mass range $m_{\text{DM}} = m_s \approx 10 - 800$ GeV if one imposes the relic density constraint. This is precisely

the mass range where the new scalar field and VL leptons can positively contribute to the $(g - 2)_\mu$ anomaly.

Interestingly, the presence of VL fermions opens up additional mechanisms for dark matter annihilation, as shown in the last diagram on the right of Fig. 2. The limits from direct detection searches can be then easily evaded, thanks to the leptophilic nature of the interaction between the dark matter scalar and the SM. By borrowing a term often used in supersymmetry, we will hence refer to this mechanism as the *bulk*. (See, e.g, Refs. [43, 44] for a definition of the bulk in supersymmetry, [45] in the context of simplified models, and [30, 46] in relation to $(g - 2)_\mu$.)

We will see in what follows that, once the new fermions are introduced in the theory to explain the $(g - 2)_\mu$ anomaly, the bulk emerges in the vast majority of cases as the favored mechanism for the dark matter relic density. However, we leave in our numerical scans the portal parameters of the scalar potential free to float, as they are allowed by the symmetries and can be constrained to small values case by case by the phenomenology. Besides, this also allows us to investigate regions of the parameter space characterized by a mixed bulk/portal mechanism for dark matter.

For the nature of the VL fermions, we consider all possibilities allowed by the SM gauge symmetry:

Model 1: Fermion singlets.

In the first class of models we add a pair of charged lepton SU(2) singlets,

$$E : (\mathbf{1}, \mathbf{1}, -1), \quad E' : (\mathbf{1}, \mathbf{1}, 1), \quad (15)$$

which are odd under \mathbb{Z}_2 . We can write new muophilic Weyl terms in the Lagrangian,

$$\mathcal{L} \supset -Y_S E e_R^* s - M_E E' E + \text{h.c.}, \quad (16)$$

in terms of a new Yukawa coupling to the second generation, Y_S , and a new VL mass, M_E .

One can also construct a new Dirac spinor, $\psi_{\tilde{E}} = (E, E'^*)^T$, which leads to the Dirac-type interaction

$$\mathcal{L} \supset -Y_S \bar{\psi}_{\tilde{E}} P_R \psi_e s + \text{h.c.}, \quad (17)$$

with $P_R = (1 + \gamma_5)/2$.

From Eq. (17) one can immediately read off the scalar and pseudoscalar couplings of Eq. (1): $g_s = Y_S/2$ and $ig_p = Y_S/2$. Alternatively, one can use the chiral formalism defined before Eq. (5) and get $c_L = 0$, $c_R = Y_S$, which can be then plugged in to calculate $\delta(g - 2)_\mu$. Since in this scenario the amplitude is not enhanced by a chirality-flip term one expects to fit the $(g - 2)_\mu$ anomaly either in the presence of large Y_S values, or with relatively small mass for the new scalar and fermion particles.

We subject Model 1, and all the models we define in the next paragraphs and sections, to several constraints from different experiments, which we describe in detail in Sec. 4. This will allow us to systematically discriminate which region of the parameter space is more likely to give a signature in future $(g - 2)_\mu$ experiments, within the individual model themselves and in relation to the others.

The constraints we consider in Model 1 are

- LHC 13 TeV bounds from searches for leptons and missing E_T [47]

- LHC 13 TeV mono-jet search bounds [48]
- EWPO constraints from the Z lineshape and asymmetry data at LEP and measurements of the muon lifetime and W mass [49]
- Where applicable (portal couplings), direct detection constraints from LUX [50] and XENON1T [42].

Model 2: Fermion doublets.

One can instead add to the Lagrangian a VL pair of SU(2) doublets,

$$L : (\mathbf{1}, \mathbf{2}, -1/2), \quad L' : (\mathbf{1}, \mathbf{2}, 1/2), \quad (18)$$

where we explicitly write the doublets as $L = (N_1, E_1)^T$ and $L' = (E_2, N_2)^T$. The heavy Dirac lepton of charge -1 is given, similarly to Model 1, by $\psi_E = (E_1, E_2^*)^T$, and there is also a heavy Dirac neutrino, whose mass is at the tree level degenerate with the charged lepton's.

As before we write new muophilic Weyl terms,

$$\mathcal{L} \supset -Y_D L' l s - M_L L' L + \text{h.c.} \quad (19)$$

or, explicitly,

$$\mathcal{L} \supset -Y_D E_2 e_L s - Y_D N_2 \nu_L s + \text{h.c.}, \quad (20)$$

which lead to the same type of Dirac interaction with muons as in Eq. (17):

$$\mathcal{L} \supset -Y_D \bar{\psi}_E P_L \psi_e s + \text{h.c.}, \quad (21)$$

where $P_L = (1 - \gamma_5)/2$. As before, one can read off $g_s = Y_D/2$, $-ig_p = Y_D/2$, or $c_L = Y_D$, $c_R = 0$. The effect on the calculation of $(g - 2)_\mu$ ends up being the same as in Model 1.

Model 3. Fermion singlets and fermion doublets.

The most straightforward way of introducing a chirality-flip term in the $(g - 2)_\mu$ calculation is letting the singlet and doublet fermions of Model 1 and Model 2 mix with each other through the SM Higgs vev.

One can thus write down

$$\mathcal{L} \supset -Y_S E e_R^* s - Y_D L' l s - \tilde{Y}_1 \phi^c L E' - \tilde{Y}_2 L' \phi E - M_E E' E - M_L L' L + \text{h.c.}, \quad (22)$$

where, in agreement with the SM and \mathbb{Z}_2 symmetries, we have introduced two additional Yukawa couplings to the Higgs boson, \tilde{Y}_1 and \tilde{Y}_2 , and again $\phi^c = -i\sigma_2 \phi^*$.

There are now two, charged, heavy Dirac leptons, and their mass matrix in the basis $\{(E_2, E') \times (E_1, E)^T\}$ is given by

$$M_C = \begin{pmatrix} M_L & \frac{\tilde{Y}_2 v}{\sqrt{2}} \\ \frac{\tilde{Y}_1 v}{\sqrt{2}} & M_E \end{pmatrix}, \quad (23)$$

and is diagonalized in the usual way by two unitary matrices U and V , with the convention that $\text{diag}(m_{E_1}, m_{E_2}) = U^* M_C V^\dagger$.

For each heavy lepton, $E_{i=1,2}^p$, the product $c_L^i c_R^{i*}$ depends on the mixing parameters:

$$\begin{aligned} c_L^i c_R^{i*} &= -Y_D V_{i1} Y_S U_{i2} \\ &\approx Y_D Y_S \frac{\max(M_L, M_E) M_{C\{ij\}} + \min(M_L, M_E) M_{C\{ji\}}}{m_{E_j^p}^2 - m_{E_i^p}^2} \Big|_{j \neq i}, \end{aligned} \quad (24)$$

where the second line of Eq. (24) is given in terms of $M_{C\{12\}} = \tilde{Y}_2 v / \sqrt{2}$ and $M_{C\{21\}} = \tilde{Y}_1 v / \sqrt{2}$. Note that $c_L^i c_R^{i*}$ vanishes when *both* \tilde{Y}_1 and \tilde{Y}_2 are zero, thus reproducing the limit of Models 1 and 2.

We subject Model 3 to the constraints described above for Model 1. Since the explicit mixing terms of Eq. (22) break chiral symmetry, we expect the constraints from EWPOs to bite significantly into the parameter space that produces an enhancement in $\delta(g-2)_\mu$. Note also that by introducing a source of chiral symmetry breaking this terms potentially induce large loop corrections to the muon mass. However, as was pointed out in, e.g., [46] for the equivalent supersymmetric case, these first order corrections do not depend on the cut-off scale and can be simply treated as a mild source of fine tuning, which should be minimal after the constraints from EWPOs are taken into account.

3.2 Models with a complex neutral scalar singlet

We extend the models of Sec. 3.1 by replacing the real scalar field of Eq. (12) with a complex scalar. We define $S = (s + ia)/\sqrt{2}$, expressed in terms of 2 real degrees of freedom.

The \mathbb{Z}_2 symmetric scalar potential now reads,

$$\begin{aligned} V &= -\mu^2 \phi^\dagger \phi + \lambda/2 (\phi^\dagger \phi)^2 + \mu_S^2/2 |S|^2 + \lambda_S/2 |S|^4 + \lambda_{12} |S|^2 \phi^\dagger \phi \\ &\quad + (\mu_S'^2/2 S^2 + \lambda_S'/2 S^4 + \lambda_{12}' S^2 \phi^\dagger \phi + \lambda_{22}'/2 S^2 |S|^2 + \text{h.c.}), \end{aligned} \quad (25)$$

where we have introduced new portal couplings, λ_{12}' and λ_{22}' , which again we leave free to float but will not play an important role in the dark matter discussion.

Tree-level vacuum stability requires in this case $\lambda > 0$, $\tilde{\lambda}_s > 0$, $\tilde{\lambda}_a > 0$, $\lambda_S > -1/6\sqrt{\tilde{\lambda}_a \tilde{\lambda}_s}$, $\lambda_{12} - 2\lambda_{12}' > -\sqrt{\lambda \tilde{\lambda}_a}$, and $\lambda_{12} + 2\lambda_{12}' > -\sqrt{\lambda \tilde{\lambda}_s}$, where $\tilde{\lambda}_s = \lambda_S + 2\lambda_S' + 2\lambda_{22}'$, $\tilde{\lambda}_a = \lambda_S + 2\lambda_S' - 2\lambda_{22}'$. The \mathbb{Z}_2 symmetry is preserved if $\mu_S^2 - 2\mu_S'^2 > 0$ and $\mu_S^2 + 2\mu_S'^2 > 0$.

The masses of dark sector scalars are given at the tree level by

$$\begin{aligned} m_s^2 &= \frac{1}{2}(\mu_S^2 + \lambda_{12} v^2 + 2\mu_S'^2 + 2\lambda_{12}' v^2) \\ m_a^2 &= \frac{1}{2}(\mu_S^2 + \lambda_{12} v^2 - 2\mu_S'^2 - 2\lambda_{12}' v^2). \end{aligned} \quad (26)$$

Thus, this scenario is endowed with two possible dark matter candidates, a scalar and a pseudoscalar WIMP (see, e.g., [51, 52] for early studies of the complex scalar/Higgs portal).

By mirroring the models of Sec. 3.1, we introduce **Model 1a**, **Model 2a**, and **Model 3a**, obtained by performing in the Lagrangians of Eqs. (16), (19), and (22) the substitutions $s \rightarrow S$ and $s \rightarrow S^*$. For example, Model 1a is characterized by the Lagrangian

$$\mathcal{L} \supset -Y_S E e_R^* S - Y_{S^*} E e_R^* S^* - M_E E' E + \text{h.c.}, \quad (27)$$

from which one reads the chiral couplings of the muon to the scalar and pseudoscalar fields: $c_R^{(s)} = (Y_S + Y_{S^*})/\sqrt{2}$, which can become significant even within the perturbativity bound for the individual Yukawa couplings, and $c_R^{(a)*} = i(Y_S - Y_{S^*})/\sqrt{2}$, which instead, being expressed as a difference, is in general a bit smaller. Besides, $c_L^{(s)} = c_L^{(a)} = 0$ like in the model with a real scalar.

Similar arguments apply to the corresponding extensions of Models 2 and 3 of Sec. 3.1. In particular, in Model 3a, we mirror the singlet/doublet fermion mixing of Model 3 by adding 2 additional Yukawa couplings, which have the effect of broadly opening up the parameter space, and making it more difficult to constrain.

We conclude this subsection by pointing out that we do not treat in this work models with charged scalar singlet fields and neutral fermions only, as in their simplest implementation they provide a negative contribution to $\delta(g - 2)_\mu$, see Eq. (6). We shall see in subsequent sections, however, that in the presence of neutral fermion mixing the second term of Eq. (6) can provide a positive contribution to $(g - 2)_\mu$.

3.3 Models with a scalar doublet

Finally, we consider models with an inert scalar doublet in place of the inert scalar singlet of Sec. 3.1 and Sec. 3.2. We introduce

$$\Phi : (\mathbf{1}, \mathbf{2}, 1/2), \quad (28)$$

where $\Phi = (S^+, S^0/\sqrt{2})^T$ in terms of a charged scalar field S^\pm and a neutral complex $S^0 = s + ia$.

At the tree level the scalar potential reads,

$$\begin{aligned} V = & -\mu^2 \phi^\dagger \phi + \lambda/2 (\phi^\dagger \phi)^2 + \mu_\Phi^2/2 \Phi^\dagger \Phi + \lambda_\Phi/2 (\Phi^\dagger \Phi)^2 \\ & + \lambda_3 \Phi^\dagger \Phi \phi^\dagger \phi + \lambda_4 (\Phi^\dagger \phi)(\phi^\dagger \Phi) + (\lambda_5 (\Phi^\dagger \phi)^2 + \text{h.c.}). \end{aligned} \quad (29)$$

Vacuum stability requires $\lambda > 0$, $\lambda_\Phi > 0$, $\lambda_3 > -\sqrt{\lambda\lambda_\Phi}$, and $\lambda_3 + \lambda_4 \pm 2\lambda_5 > -\sqrt{\lambda\lambda_\Phi}$, as well as $\mu_\Phi^2 > 0$.

At the tree level the masses of dark sector scalars are given by

$$\begin{aligned} m_s^2 &= \frac{1}{2}\mu_\Phi^2 + \frac{1}{2}v^2(\lambda_3 + \lambda_4 + 2\lambda_5) \\ m_a^2 &= \frac{1}{2}\mu_\Phi^2 + \frac{1}{2}v^2(\lambda_3 + \lambda_4 - 2\lambda_5) \\ m_{S^\pm}^2 &= \frac{1}{2}(\mu_\Phi^2 + v^2\lambda_3). \end{aligned} \quad (30)$$

As a consequence, the dark matter can be either a scalar or pseudoscalar, but additional constraints on the parameter space arise from the condition that the charged scalar is not the lightest one, and it evades the LEP limit, $m_{S^\pm} > 100 \text{ GeV}$. The portal interactions and dark matter of this class of models have been investigated extensively (early studies include [53–57]) but, once more, in most of the cases described here the relevant mechanism for the relic density will be provided by the bulk.

The fermion fields can in this case be grouped in 4 categories according to their SU(2) representation: singlet, doublet, triplet, and adjoint triplet. As before, we also consider the possibility of doublet/singlet mixing and doublet/triplet mixing through the Higgs vev.

Model 4. Fermion singlets.

In terms of the singlets defined in Eq. (15) the Lagrangian reads

$$\mathcal{L} \supset -Y_S \Phi^c l E' - M_E E E' + \text{h.c.}, \quad (31)$$

where we have introduced, with some redundancy in the notation, a new Yukawa coupling, Y_S , and VL mass, M_E . Writing explicitly the components of the SM doublet, one gets

$$\mathcal{L} \supset -Y_S \left(\nu_L S^- E' + e_L \frac{S^{0*} E'}{\sqrt{2}} \right), \quad (32)$$

which gives $c_L^{(s)} = Y_S/\sqrt{2}$, $c_L^{(a)} = -iY_S/\sqrt{2}$, and $c_R^{(s,a)} = 0$. Note that even though the chiral structure of Eq. (32) resembles the scalar singlet case of Model 1a, the presence of a non-zero coupling of VL fermions to muon neutrinos will have an important impact on the LHC phenomenology.

Model 5. Fermion doublets.

For the VL doublets introduced in Eq. (18), the Lagrangian reads

$$\mathcal{L} \supset -Y_D \Phi^c L e_R^* - M_L L' L + \text{h.c.}, \quad (33)$$

in terms of a new Yukawa coupling, Y_D , and VL mass, M_L .

Beside a positive contribution to $(g-2)_\mu$, similar to Eq. (32) and Eq. (20), there is a negative contribution due to the charged scalar field,

$$\mathcal{L} \supset -Y_D \left(N_1 S^- e_R^* + \frac{E_1 S^{0*}}{\sqrt{2}} e_R^* \right) + \text{h.c.} \quad (34)$$

This feature suggests that boosting $(g-2)_\mu$ to the experimentally measured value may be more challenging in this case, see Eq. (6).

Model 6. Fermion singlets and fermion doublets.

The fermion doublets of Model 5 can mix with the singlets of Model 4 through the Higgs boson vev. The Lagrangian includes the terms

$$\mathcal{L} \supset -Y_S \Phi^c l E' - Y_D \Phi^c L e_R^* - \tilde{Y}_1 \phi^c L E' - \tilde{Y}_2 L' \phi E + \text{h.c.}, \quad (35)$$

with two additional Yukawa couplings, in a fashion similar to Model 3 in Sec. 3.1.

Note, however, that even if the mixing provides a source of chiral symmetry breaking similar to the one giving a boost to $(g-2)_\mu$ in Model 3, we do not expect an enhancement in this model. The reason is that there are two neutral real scalar fields, s and a , whose couplings to the muon have opposite parity but the same size. One can read off from Eqs. (32) and (34) that $c_L^{(a)} = -i c_L^{(s)}$ and $c_R^{(a)*} = -i c_R^{(s)*}$, so that $\Re(c_L^{(a)} c_R^{(a)*}) = -\Re(c_L^{(s)} c_R^{(s)*})$ and the last term in Eq. (5) is identically zero. As a consequence, Model 6 does not result much more

interesting from a phenomenological point of view than the individual models comprising it, and we do not consider it further.

Model 7. Fermion triplets.

In this case one extends the SM by adding fermion SU(2) triplets with the following quantum numbers,

$$\Psi_T : (\mathbf{1}, \mathbf{3}, -1), \quad \Psi'_T : (\mathbf{1}, \bar{\mathbf{3}}, 1), \quad (36)$$

which can be parameterized in terms of a neutral, charged, and doubly charged component as

$$\Psi'_T = \begin{pmatrix} \frac{\Psi^+}{\sqrt{2}} & \Psi^{++} \\ \Psi^0 & -\frac{\Psi^+}{\sqrt{2}} \end{pmatrix},$$

and equivalent decomposition applies to Ψ_T .

The Lagrangian reads

$$\mathcal{L} \supset -Y_T \Psi'_T \Phi^c l - M_T \text{Tr}(\Psi'_T \Psi_T) + \text{h.c.} \quad (37)$$

which is expanded into

$$\mathcal{L} \supset -Y_T \left(\frac{\Psi^+ S^{0*}}{2} + \Psi^{++} S^- \right) e_L - Y_T \left(\frac{\Psi^0 S^{0*}}{\sqrt{2}} + \frac{\Psi^+ S^-}{\sqrt{2}} \right) \nu_L + \text{h.c.} \quad (38)$$

Equation (38) includes the well-known doubly-charged fermion/charged scalar coupling, which will generate the large positive contribution to $(g-2)_\mu$ given in Eq. (9).

Note that in this case too, the quantum numbers allow for doublet/triplet fermion mixing through the Higgs vev. As in the case just discussed above, however, the couplings of s and a to the muon have opposite parity and equal size, providing, again, an identical cancellation of the chirality-flip term.

Model 8. Fermion adjoint triplet.

If the hypercharge of the VL fermion is zero, one obtains an adjoint SU(2) triplet:

$$\Psi_A : (\mathbf{1}, \mathbf{3}, 0) \quad (39)$$

where the triplet's matrix form is

$$\Psi_A = \begin{pmatrix} \frac{\Psi^0}{\sqrt{2}} & \Psi^+ \\ \Psi^- & -\frac{\Psi^0}{\sqrt{2}} \end{pmatrix},$$

in terms of a charged fermion and a neutral Majorana field.

The Lagrangian in this scenario reads

$$\mathcal{L} \supset -Y_A \Phi \Psi_A l - M_A \text{Tr}(\Psi_A \Psi_A) + \text{h.c.} \quad (40)$$

This gives

$$\mathcal{L} \supset -Y_A \left(\frac{\Psi^0 S^+}{\sqrt{2}} + \frac{\Psi^+ S^0}{\sqrt{2}} \right) e_L - Y_A \left(\frac{\Psi^0 S^0}{2} - \Psi^- S^+ \right) \nu_L + \text{h.c.} \quad (41)$$

Like in Model 5, there is here a negative contribution to $(g - 2)_\mu$ arising from the coupling of the muon with the charged scalar.

Model 9. Fermion adjoint triplet and fermion doublets.

Positive contributions to $(g - 2)_\mu$ arise in case the adjoint fermion triplet mixes with the doublet through the SM Higgs vev. As before, we add to the Lagrangian

$$\mathcal{L} \supset -\tilde{Y}_1 \Psi_A L \phi - \tilde{Y}_2 \Psi_A L' \phi^c + \text{h.c.} \quad (42)$$

Note that, besides the mixing between two heavy charged fermions, Eq. (42) leads to the additional presence of two heavy neutral fermions mixing with each other. The chirality-flip contribution to $(g - 2)_\mu$ is not suppressed in this case as, on the one hand, $c_L^{(a)} = i c_L^{(s)}$ and $c_R^{(a)*} = -i c_R^{(s)*}$, and on the other there is an additional positive-value loop involving the heavy mixing “neutrinos”, see the last term in Eq. (6).

We conclude this section by pointing out that we do not treat cases with scalar SU(2) triplets in this work. The reason is twofold. On the one hand, it was pointed out in Ref. [27] that in some cases (scalar triplet/fermion doublets, scalar adjoint triplet/fermion doublets, and scalar triplet/fermions adjoint-triplet and singlet) the 1-loop contribution to $(g - 2)_\mu$ is negative. On the other hand, even for the cases where a positive contribution exists (scalar adjoint triplet/fermions triplet and singlet), the correct dark matter relic density can only be obtained with the scalar mass in the range of 5.5 TeV [58], which is obviously too high to accommodate the anomaly.

4 Experimental constraints

We review in this section the experimental constraints that can affect the allowed parameter space of the BSM models introduced in Sec. 3.

4.1 Electroweak precision observables

We subject all our models to electroweak precision constraints. Since VL fermions do not have tree-level axial-vector couplings, their contribution to EWPOs is expected to be small. However, in the models with mixing between fermions of different representations, and in models with scalar multiplets whose components are not mass-degenerate, loop-induced effects can be significant.

In this work we compare to the experimental data two observables. We calculate the $Z\mu\bar{\mu}$ effective coupling and confront the result with precision fits for g_A and g_V from the Z lineshape and asymmetry data at LEP and SLC [59], as reported by the PDG [49]. We also confront the corrections to the W mass with its measured value.

To calculate loop corrections to the $Z\mu\bar{\mu}$ couplings and W mass we follow the formalism of [60], which was adopted in, e.g., [61] for a precision analysis of supersymmetry. The conventions for Passarino-Veltman functions are also taken from [60,61] and we use `LoopTools` [62] for their calculation. The impact of precision observables in models with VL fermions for the $(g - 2)_\mu$ anomaly has been also recently investigated in [34].

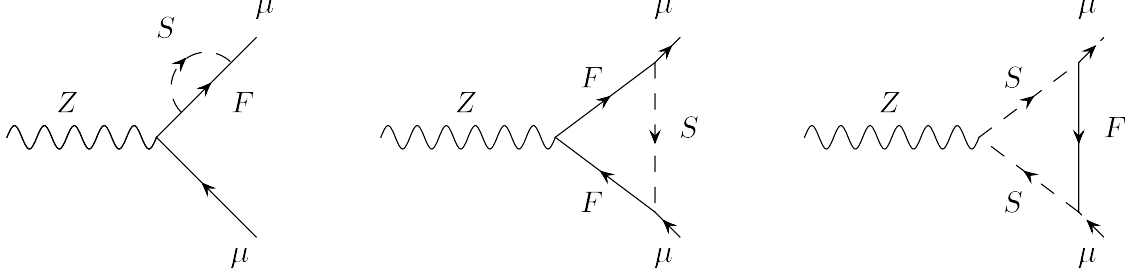


Figure 3: One-loop BSM contribution to the $Z\mu\bar{\mu}$ vertex in extensions of the SM with a generic new fermion F and a scalar S .

1. Oblique parameters.

Oblique parameters S , T and U [63] capture the BSM contributions to the gauge bosons' vacuum polarization. S is related to the difference between the number of the left- and right-handed weak fermion doublets, thus providing a measure of the breaking of the axial part of $SU(2)$. This means that in the models with degenerate VL fermions the contribution to S vanishes.

The oblique parameter T is related to the difference between the Z and W bosons' self-energies, thus providing a measure of the breaking of the vector part of $SU(2)$. As a result, it is sensitive to the mass splitting between the components of an electroweak doublet [49],

$$\Delta T = \frac{1}{32\pi^2 v^2 \alpha} \sum \Delta m^2, \quad (43)$$

where α is the fine-structure constant, the sum runs over all non-degenerate doublets, and

$$\Delta m^2 = m_1^2 + m_2^2 - \frac{2m_1^2 m_2^2}{m_1^2 - m_2^2} \ln \frac{m_1^2}{m_2^2}. \quad (44)$$

In cases where VL fermions mix, as in Model 3, 3a, and 9, their contribution to the parameters S and T can be parameterized in terms of the mixing matrices and of the physical masses. When calculating these effects, we use formulas derived in Ref. [64]. A contribution to the oblique parameter U is generally much smaller and can be neglected.

2. $Z\mu\bar{\mu}$ vertex corrections.

One-loop corrections to the coupling of the Z boson with the left-handed and right-handed muon arise from diagrams like the ones depicted in Fig. 3. They are given by

$$\Delta g_{L,R}^\mu = \frac{1}{\sqrt{4\sqrt{2}G_F M_Z^2}} [g_{L,R}^{\text{SM}} \Sigma'_{L,R}(0) - \Gamma_{L,R}(M_Z^2)], \quad (45)$$

where the Σ' terms are the derivatives of the self-energy functions of the external fermion legs at zero momentum, $\Gamma_{L,R}(M_Z^2)$ arises from triangular vertex corrections, and $g_{L,R}^{\text{SM}} = (-\hat{s}_W^2 Y + \hat{c}_W^2 T_3) g/c_W$.

In terms of Passarino-Veltman functions the Σ' terms read

$$\Sigma'_{L,R}(0) = \frac{1}{16\pi^2} \left[\sum_{F_i, S_j} |c_{L,R}^{ij}|^2 (B_0 + B_1)(0; m_{S_j}, m_{F_i}) \right], \quad (46)$$

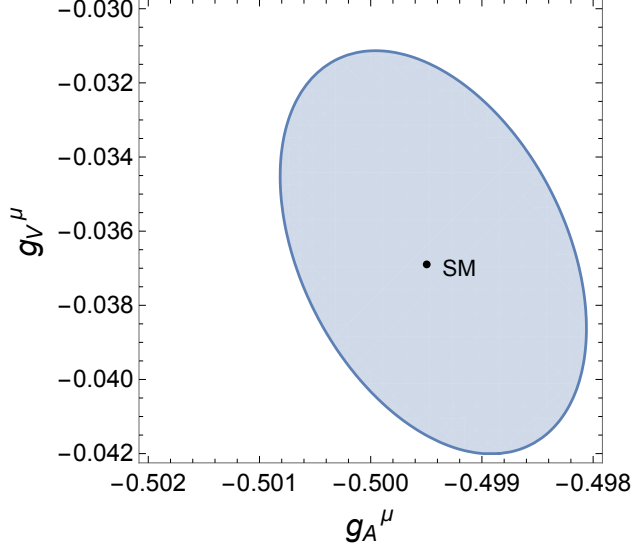


Figure 4: An estimate of the 95% C.L. region in g_A^μ , g_V^μ from a fit of Z lineshape and asymmetry data at LEP and SLC [59]. The ellipse is obtained by rescaling the 39% C.L. region given in [49].

where $c_{L,R}^{ij}$, the couplings of the generic new fermion F_i and scalar S_j to the muon, are given for our models in Sec. 3.

The contributions from triangle diagrams are

$$\begin{aligned} \Gamma_{L,R}(M_Z^2) = & -\frac{1}{16\pi^2} \sum_{F_i, S_j, F_k, S_l} \left\{ c_{L,R}^{ij*} c_{L,R}^{kj} [g_{L,R}^{Zik} m_{F_i} m_{F_k} C_0(p_1, p_2 : m_{F_i}, m_{S_j}, m_{F_k}) \right. \\ & + g_{R,L}^{Zik} \left(-M_Z^2 C_{12} - M_Z^2 C_{23} - 2C_{24} + \frac{1}{2} \right) (p_1, p_2 : m_{F_i}, m_{S_j}, m_{F_k}) \Big] \\ & \left. - c_{L,R}^{ij*} c_{L,R}^{il} g^{Zjl} 2 C_{24}(p_1, p_2 : m_{S_j}, m_{F_i}, m_{S_l}) \right\}, \quad (47) \end{aligned}$$

where the $g_{R,L}^{Zik}$ and g^{Zjl} give the SM-like couplings of the Z to the new fermions and scalars.

After evaluating the observable couplings $g_V^\mu = g_L^\mu - g_R^\mu$ and $g_A^\mu = g_L^\mu + g_R^\mu$ from $g_L^\mu \equiv -0.2682 + \Delta g_L^\mu$ and $g_R^\mu \equiv 0.2313 + \Delta g_R^\mu$, we compare them to the 95% C.L. contour presented in Fig. 4, which we have approximately determined by rescaling up the 39% C.L. contour given in [49].

We also confront all our models with rough estimates of the reach in the possible future high-precision experiments GigaZ [65], with an estimated improvement of a factor 20 [66] in the systematic uncertainty, and TLEP [67], with an improvement of a factor 100.

2. Constraints from the W mass.

Additionally, we calculate the corrections to the W mass in our models. We follow, again, Refs. [60, 61], which parameterize

$$M_W = M_W^{\text{SM}} + \Delta M_W \quad (48)$$

$$\Delta M_W = -0.288\Delta S + 0.418\Delta T + 0.337\Delta U - 0.126\frac{\Delta\bar{\delta}_G}{\bar{\alpha}}, \quad (49)$$

in terms of the usual oblique parameters S , T , U . We use $M_W^{\text{SM}} = 80.361 \text{ GeV}$ and $\bar{\alpha}^{-1} = 127.95$. We neglect ΔU , which is small, and we calculate the corrections to the S and T parameters using analytic formulas of Ref. [64] for the fermions, and of Ref. [53] for the scalars.

We calculate $\Delta\bar{\delta}_G = 2\delta^v$, the correction to the muon lifetime, as

$$\delta^v = \frac{\sqrt{2}}{\hat{g}} \Gamma^{W\mu\nu\mu}(0) - \frac{1}{2} \left[\Sigma'_{\mu_L}(0) + \Sigma'_{\nu_\mu}(0) \right], \quad (50)$$

where \hat{g} is the \overline{MS} value of the weak coupling constant and, once more, Σ' and $\Gamma^{W\mu\nu\mu}$ parameterize corrections to the external legs and triangle diagrams modifying the $W\mu\nu_\mu$ vertex.

When expressed in terms of the Passarino-Veltman functions they are given by

$$\Sigma'_{\mu_L, \nu_\mu}(0) = \frac{1}{16\pi^2} \sum_{F_i, S_j} |c_L^{ij}|^2 (B_0 + B_1)(0; m_{S_j}, m_{F_i}) \quad (51)$$

and

$$\begin{aligned} \Gamma^{W\mu\nu\mu}(0) = \frac{1}{16\pi^2} \sum_{F_i, S_j, F_k, S_l} \left\{ -c_L^{ij*} c_L^{kj} \left[g_L^{W ik} m_{F_i} m_{F_k} C_0(0; m_{F_i}, m_{S_j}, m_{F_k}) \right. \right. \\ \left. \left. + g_R^{W ik} \left(-2C_{24} + \frac{1}{2} \right) \right] (0; m_{F_i}, m_{S_j}, m_{F_k}) + c_L^{ij*} c_L^{il} g^{W jl} 2C_{24}(0; m_{S_j}, m_{F_i}, m_{S_l}) \right\}, \quad (52) \end{aligned}$$

where the symbols have equivalent meaning as in Eq. (47).

4.2 Collider constraints

In all our models, we apply a default hard cut on the mass of new charged particles, $m_{E^\pm, S^\pm} > 100 \text{ GeV}$ to roughly take into account LEP II limits.

Moreover, since the VL fermions are charged under the SM electroweak gauge symmetry group, they can be pair-produced at the LHC in Drell-Yan processes, $pp \rightarrow Z, \gamma, W^\pm \rightarrow F \bar{F}$, and subsequently undergo Yukawa-driven decays into a DM scalar and a muon, $F \rightarrow S \mu$, thus leading to a characteristic 2 leptons plus missing energy (MET) signature. Such a topology has been investigated both by ATLAS and CMS in the context of supersymmetry in the searches dedicated to sleptons, charginos and neutralinos.

In this work we employ the ATLAS 2-lepton search [47] based on 13 TeV data with an integrated luminosity of 13.3 fb^{-1} . We numerically recast the experimental analysis for the models introduced in Sec. 3, following the procedure described in detail in [68, 69] and references therein. The main kinematical variable used by the collaboration to discriminate between the signal and the SM background is the transverse mass m_{T2} , with the end point correlated to the mass splitting between fermion and dark matter scalar, δm . As a result, the sensitivity of the search weakens when the mass splitting decreases, dropping to zero when $\delta m \approx 70 \text{ GeV}$.

Singlet scalar dark matter can be pair-produced at the LHC through the off-shell Higgs boson, $pp \rightarrow h^* \rightarrow S S$. The cross-section is in this case directly proportional to the size of the

portal couplings and is not expected to be significant, given the discussed stringent bounds from direct detection experiments. For doublet scalar dark matter, Drell-Yan production with electroweak-size cross section is also possible, $pp \rightarrow Z, \gamma, W^\pm \rightarrow \Phi^\dagger \Phi$. Such a signature can be probed by monojet searches, which tag an energetic jet from initial-state radiation recoiling against the produced dark matter. To capture this possibility, we recast the ATLAS 13 TeV analysis [48] with 3.2 fb^{-1} of data. Besides the present exclusion bounds, we also calculate the sensitivity of both ATLAS searches with the assumed luminosity of 300 fb^{-1} at the LHC 14 TeV run.

If $m_{DM} < m_h/2$, the Higgs boson can invisibly decay into dark matter with branching ratio proportional to the portal coupling(s). For completeness, we apply the CMS upper bound on the corresponding branching ratio, $\text{BR}(h \rightarrow \text{invisible}) < 0.24$ at the 95% confidence level [70].

Finally, we recall that we apply to all our models the relic density constraint from Planck [71], $\Omega h^2 = 0.1188 \pm 0.0010$, to which we add in quadrature a $\sim 10\%$ theoretical uncertainty, and the XENON1T 90% C.L. upper bound on the spin-independent cross section σ_p^{SI} [42] as a hard cut.

5 Numerical analysis

We present now the results of the numerical analysis of the models introduced in Sec. 3. We will start with a brief description of the numerical tools utilized in the study.

Each of the considered models has been generated with **SARAH** v.4.9.3 [72] and the corresponding **SPheno** [73, 74] modules have been produced to calculate mass spectra and decay branching ratios. Flavor observables, including $\delta(g-2)_\mu$, have been calculated with the **FlavorKit** package [75] of **SARAH-SPheno**. Model files for **CalcHEP** [76] were also generated and passed to **MicrOMEGAs** v.4.3.1 [77] to calculate dark matter related observables.

In order to efficiently scan the multidimensional parameter space, all the packages were interfaced to **MultiNest** v.3.10 [78] for sampling. We employ a Gaussian likelihood function to find the regions favored by the dark matter relic density and $\delta(g-2)_\mu$.

The parameters of the models are scanned in the following ranges:

$$\begin{aligned}
0.001 &\leq \text{Yukawa couplings} &&\leq \sqrt{4\pi}, \\
-1 &\leq \text{portal couplings} &&\leq 1, \\
100 \text{ GeV} &\leq M_{L,E,T,A} &&\leq 10000 \text{ GeV}, \\
(10 \text{ GeV})^2 &\leq \mu_s^2, \mu_S^2, \mu_\Phi^2 &&\leq (5000 \text{ GeV})^2, \\
-0.5 \mu_S^2 &\leq \mu_S'^2 &&\leq 0.5 \mu_S^2.
\end{aligned} \tag{53}$$

The LHC limits from the ATLAS 2-lepton and monojet searches has been implemented using the recast procedure described in detail in [68, 69] and adapted to handle non-SUSY scenarios. To this end, **UFO** files have been generated with **SARAH** and passed to **MadGraph5_aMC@NLO** [79], where a set of new BSM processes with a corresponding output for **PYTHIA** [80] were created. Finally, the hadronization products were passed to the fast detector simulator **DELPHES 3** [81].

We perform our numerical analysis at the tree level. In doing so, we are relying on some underlying assumptions that may not be always warranted, especially in theories including several scalar fields like the ones investigated here.

Significant loop corrections that depend on the input parameters affect the value of the scalar masses, in particular those that depend on the BSM Yukawa couplings which, as we shall see, in general have to be sizable to accommodate the experimentally measured value of $\delta(g-2)_\mu$. **SARAH** v.4.9.3 allows one to calculate 1-loop corrections to all scalar masses, and define the input parameter at a high renormalization scale of choice. However, it has been pointed out [82] that the results so implemented maintain a significant residual dependence on the renormalization scale. One should therefore make use of the full 2-loop calculation, which has only become available very recently [82].

Thus, in this work we limit ourselves to the assumption generally adopted in the literature when dealing with non-supersymmetric BSM scalar fields, i.e., that it is possible to absorb corrections to the scalar masses into the counterterms of the free parameters. Note that effects of 1-loop corrections to the scalar mass in relation to the relic density in inert scalar models have been analyzed, e.g., in [83,84]. In Ref. [84], in particular, it was shown that as long the input parameters are defined not far above the EWSB scale, say up to 10 TeV or so, the parameter space regions in agreement with the relic density are not altered drastically with respect to the tree level.

5.1 Real scalar with a singlet or doublet VL fermion

We begin our discussion with **Model 1**, characterized by the addition of a real scalar particle and VL fermion singlet fields to the spectrum of the SM. The \mathbb{Z}_2 -odd scalar plays the role of the dark matter particle in this case, and we will refer to it with $m_{\text{DM}} \equiv m_s$ interchangeably.

In Fig. 5(a) we present a plot of the model's parameter space in the plane of the new coupling to the muon, $c_R = Y_S$, versus the dark matter mass. The parameter space allowed at 2σ (including a $\sim 10\%$ theory error) by the relic density is shown in cyan, and we highlight with a darker shade the region in which $\Omega h^2 \approx 0.12$ is due with good approximation exclusively to the bulk. The $(g-2)_\mu$ constraint is shown in dark blue and we do not impose at this stage any LHC or precision constraints.

Higgs-portal dark matter plays a small role, almost exclusively limited to the region above $0.8 - 1$ TeV, in which the recent bounds from XENON1T can be evaded. Note that the relic abundance imposes a lower bound on the mass of the scalar particle, $m_s = m_{\text{DM}} \gtrsim 40 - 50$ GeV, as the bulk mechanism loses its efficiency when the spread between m_s and $m_{\tilde{E}}$ is significant (recall that $m_{\tilde{E}} \gtrsim 100$ GeV by LEP bounds). As we shall see below, this lower bound on the dark matter mass is model-dependent and can be evaded in other scenarios.

The parameter space allowed at 2σ by the combination of relic density and $(g-2)_\mu$ is shown in green. The 2σ region from the BNL measurement places an upper bound on the mass of the dark matter scalar, $m_s \lesssim 170 - 180$ GeV, beyond which one is forced to resort to non-perturbative values for the new Yukawa coupling Y_S , independently of the size of $m_{\tilde{E}} > m_s$.

In Fig. 5(b) we show the points of the allowed parameter space – the green region of Fig. 5(a) – in the $(m_{\tilde{E}}, m_{\text{DM}})$ plane, best suited for interpreting the LHC constraints. We also apply here the constraints from precision observables, which have no visible effect in

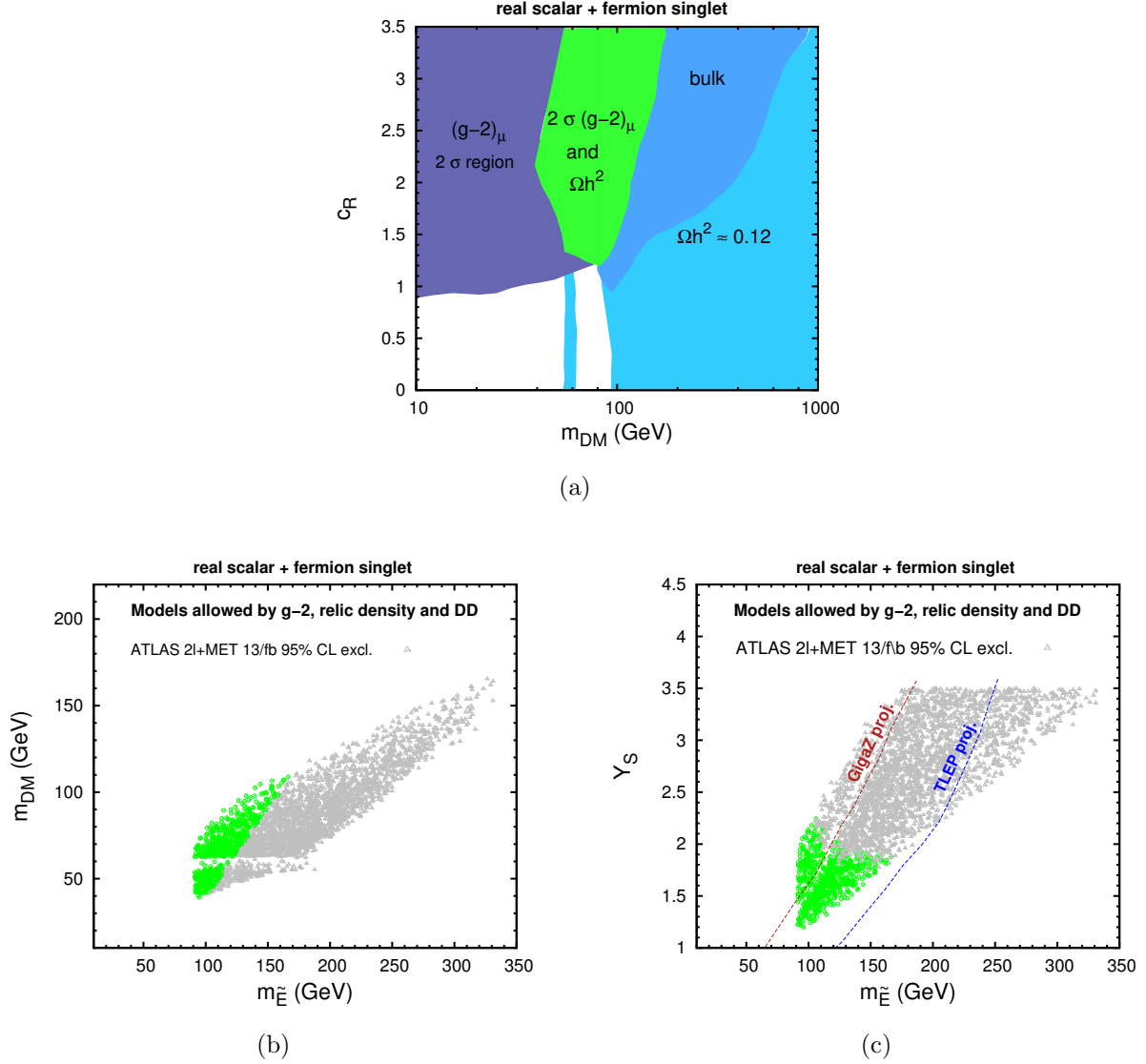


Figure 5: (a) The (m_{DM}, c_R) plane for Model 1 (real scalar field and VL fermion singlet). In cyan, the parameter space favored at 2σ by the relic density is shown, while the one favored by the $(g-2)_\mu$ measurement is shown in dark blue. Green region corresponds to those values of model parameters where both constraints are satisfied simultaneously. (b) The parameter space common to the relic density and $(g-2)_\mu$ in the $(m_{\tilde{E}}, m_{DM})$ plane. Gray triangles show the parameter space excluded by the ATLAS 2 lepton search [47]. (c) Same as (b) but in the $(m_{\tilde{E}}, Y_S)$ plane. The projected reach of precision measurements at GigaZ [65] and TLEP [67] is also shown.

this case due to the VL nature of the new fermion. The ATLAS 2-lepton + missing E_T bound is applied and the excluded points are shown with gray triangles. The bound is quite aggressive, and excludes most of the parameter space in the picture, with the exception of a limited region in which $m_{\tilde{E}}$ and m_s become increasingly close to each other, as the m_{T2} variable loses its discriminating power for compressed and semi-compressed spectra. We have

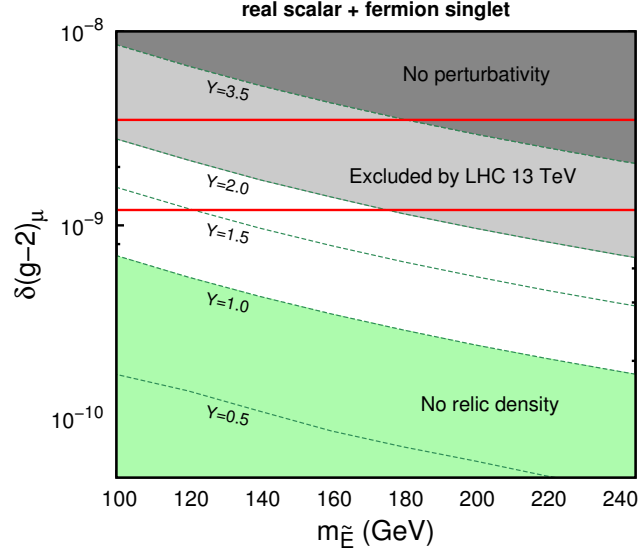


Figure 6: The measurement of $\delta(g-2)_\mu$ as a function of the VL fermion mass and the new Yukawa coupling in Model 1. The scalar dark matter mass is fixed here at $m_s = m_{\text{DM}} = 80 \text{ GeV}$, but the plot is not very sensitive to its value. The horizontal red solid lines show the 2σ region of the BNL experiment.

also calculated the reach of the ATLAS search with 300 fb^{-1} , but the latter shows little if any impact on the surviving region, due to the intrinsic ineffectiveness of m_{T_2} for these spectra. The surviving parameter space is thus likely to remain challenging for searches based on this strategy. Note, incidentally, that neither the monojet search, nor Higgs invisible decay, can provide a complementary way of testing the surviving region due to the smallness of the portal Higgs-coupling.

The same points are shown in Fig. 5(c), in the plane of the new Yukawa coupling, Y_S , versus the VL fermion mass. Because of the large Yukawa values, future precision experiments like GigaZ or TLEP, with a projected improvement by a factor 20 or more over LEP, have the potential to probe the surviving region.

We summarize the case of Model 1 in Fig. 6, where we present predictions for this model based on an eventual measurement of $(g-2)_\mu$ at Fermilab. The different bounds discussed above are applied.

Model 2, characterized by the coupling of the muon to a real scalar singlet and a fermion doublet, does not show significant differences from Model 1 at the tree level. This could have been anticipated by a simple inspection of the two Lagrangians, Eq. (16) and Eq. (19). The dark matter particle is the same in both cases and the contributions to the $(g-2)_\mu$ calculation are the same, as one can simply switch the role of c_L and c_R in Eq. (5) (and one of them is always zero). The bounds from EWPOs are easily satisfied in both models, as both lack a significant source of chiral symmetry breaking.

The LHC multi-lepton bound is in principle stronger for the fermion doublet case in the region of large m_E and small m_{DM} , due to the possibility of producing the doublet through the W boson, which enhances the cross section. However, we do not expect any difference

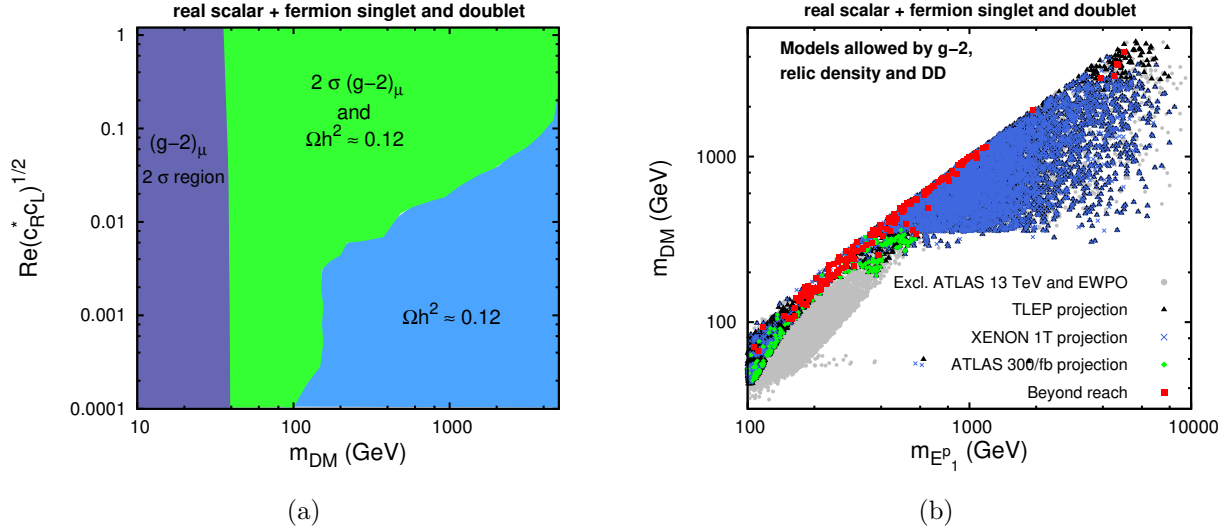


Figure 7: (a) The $[m_{\text{DM}}, \Re(c_L^1 c_R^{1*})^{1/2}]$ plane for Model 3 (real scalar field and mixing singlet and doublet VL fermions). The color code is the same as in Fig. 5(a). (b) The parameter space of Model 3 in agreement with the relic density and the $(g-2)_\mu$ anomaly at 2σ in the $(m_{E_1^p}, m_{\text{DM}})$ plane. Gray dots are excluded by a combination of electroweak precision data and the ATLAS 2 leptons + MET search at 13 TeV. The projected reach of the ATLAS search with 300 fb^{-1} probes the points shown as green dots; new data from XENON-IT will test the points shown as royal-blue crosses; and improved electroweak precision at TLEP will test the points marked by black triangles. The points shown as red squares are possibly outside of foreseeable reach.

from what is shown in Fig. 5(b), as the limit is strong enough to exclude this region in Model 1 as well. Thus, no difference can be observed between Model 1 and Model 2, and the reader can refer to Figs. 5 and 6 for Model 2 as well.

5.2 Real scalar with mixing singlet and doublet VL fermions

As was discussed in Sec. 3.1, when the singlet and doublet fermion are both included in the theory, they can mix through the Higgs boson field vev. This introduces an explicit source of chiral-symmetry violation, which can boost the $(g-2)_\mu$ value as now both c_L and c_R differ from zero in Eq. (5). For the same reason, however, this model, which we dubbed **Model 3**, is also subject to strong constraints from EWPOs.

We present in Fig. 7(a) the parameter space of Model 3 in the $[m_{\text{DM}}, \Re(c_L^1 c_R^{1*})^{1/2}]$ plane, without for the moment applying the limits from EWPOs and the LHC. The color code is the same as in Fig. 5(a). The $(g-2)_\mu$ anomaly can be accommodated for very large dark matter mass, well into the TeV range, thanks to the above-mentioned boost provided by the chirality-flip term involving $c_L c_R$. For the same reason, the new Yukawa couplings are also allowed to span a broader range, with the sum of them being as small as ~ 0.2 .

We show the points of the parameter space favored by Ωh^2 and $(g-2)_\mu$ in the $(m_{E_1},$

m_{DM}) plane in Fig. 7(b). After applying the remaining constraints, we mark with gray dots the points excluded by a combination of the ATLAS 2-lepton + MET search (mostly on the bottom left) and EWPOs (mostly on the top right). Electroweak precision bounds exclude solutions with large fermion mass as large singlet/doublet mixing is required to fit the $(g-2)_\mu$ constraint at 2σ .

More specifically, the BSM contributions to the $Z\mu\bar{\mu}$ vertex imply $\Re(c_L^1 c_R^{1*})^{1/2} \lesssim 0.01$, unless both Yukawa couplings are close in value. In that case the limit weakens to $\Re(c_L^1 c_R^{1*})^{1/2} \lesssim 0.1$. On the other hand, the corrections to the W mass, which arise from BSM contributions to the muon lifetime and the oblique parameters, test two distinctive regions of the parameter space: the small mass regime, with $m_s < 100$ GeV and a small fermion mixing, where the corrections to muon decay are dominant; and the large mass regime, in which the large mixing induces large splitting of the doublet fermion masses, which subsequently increase the parameter T .

The points that are not excluded by LEP or the recent LHC constraints are in reach of the high-luminosity LHC or future experiments sensitive to corrections to the $Z\mu\bar{\mu}$ effective coupling. The points in reach of the LHC with 300 fb^{-1} are shown as green diamonds, whereas black triangles mark the points in reach of future precision experiments. Note that points characterized by a non-negligible portal coupling, $\lambda_{12} \gtrsim 0.1$, will be tested in complementarity with the next release from XENON-1T data, and we show these points in Fig. 7(b) as royal-blue crosses. Finally, we highlight with red squares the points that appear to be beyond the reach of all of the projected measurements considered in this work.

We point out that these points are almost all characterized by the scalar and lightest fermion mass being very close to each other. This is not enforced by any of the symmetries of the Lagrangian considered in Sec. 3.1, so that we can conclude that Model 3 requires a certain amount of fine tuning to evade all future bounds.

5.3 Complex singlet scalar with VL fermions

In Fig. 8(a) we present the parameter space of **Model 1a** in the $(m_{\text{DM}}, c_R^{(s)})$ plane (recall that $c_R^{(s)} = (Y_S + Y_{S^*})/\sqrt{2}$). At this stage the LHC and precision constraints have not been yet applied, and the color code is the same as in Fig. 5(a), with the only difference being that we do not explicitly highlight here the parameter space region belonging to the bulk.

The most striking difference with Model 1 is that in Model 1a one can fit the $(g-2)_\mu$ anomaly with lighter dark matter, as light as our prior range allows, $m_s, m_a \approx 10$ GeV. This is due to the presence of two possible dark matter particles in this mass range, the scalar s and the pseudoscalar a . When their masses are not far apart from one another, the relic density can be effectively diluted in the early Universe thanks to additional bulk processes like $a s \rightarrow \mu^+ \mu^-$, or $a a \rightarrow \mu^+ \mu^-$.

When one applies the constraints from the LHC (precision bounds do not alter the picture much in this model) the available parameter space is much reduced. We project the region favored by a combination of the relic density and $(g-2)_\mu$ constraints to the plane $(m_{\tilde{E}}, c_R^{(s)})$. The result is presented in Fig. 8(b). The region in gray is excluded by the LHC 2-lepton search. We also show with dashed lines of different colors the projected reach of the LHC with 300 fb^{-1} , and of future precision experiments at GigaZ and TLEP.

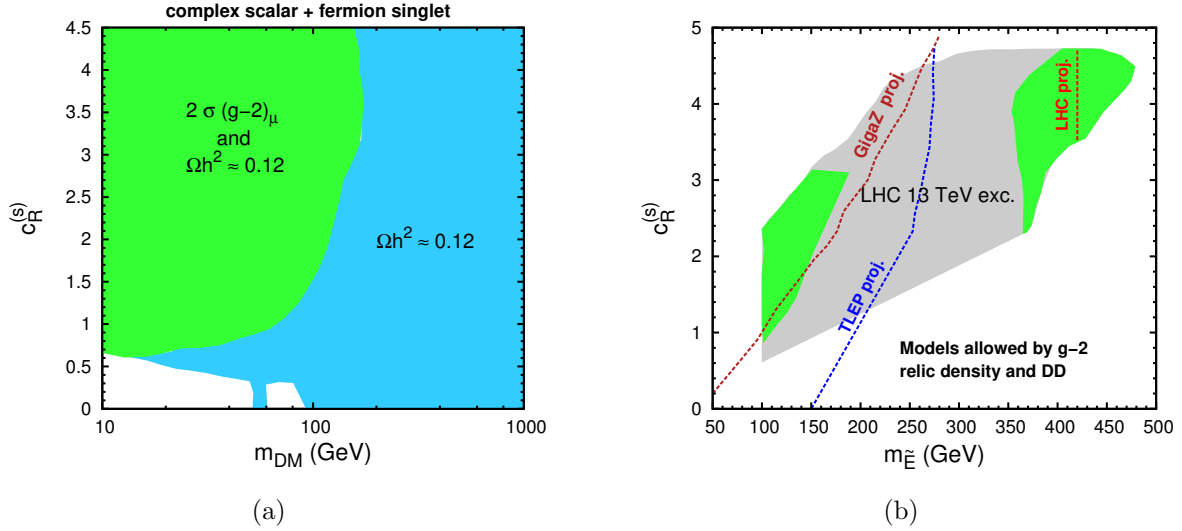


Figure 8: (a) The $(m_{\text{DM}}, c_R^{(s)})$ plane for Model 1a (complex scalar field and singlet VL fermions). The color code is the same as in Fig. 5(a). (b) Region of Model 1a favored by a combination of the relic density and $(g-2)_\mu$ constraints in the plane $(m_{\tilde{E}}, c_R^{(s)})$. The gray area is excluded by the LHC 2-lepton + MET search. Projected reach at the LHC with 300 fb^{-1} , and future precision experiments at GigaZ and TLEP, are shown as dashed lines.

As dark matter particles, the scalars s and a behave symmetrically, with the only difference being that, by construction, the available range for the coupling of s to the muon, $c_R^{(s)} = (Y_S + Y_{S^*})/\sqrt{2}$, is slightly larger than the allowed coupling for a , $|c_R^{(a)}| = |Y_S - Y_{S^*}|/\sqrt{2}$. In fact, the region with good dark matter in Fig. 8(a) features solutions of various types, $m_s \approx m_a$, $m_s \ll m_a$, $m_a \ll m_s$, and cases in between.

Because of a quite large number of free parameters, however, a measurement of $(g-2)_\mu$ is not sufficient in Model 1a to pinpoint specific features and correlations of some parameters with respect to others. Thus, we identify two limiting cases that we show in Fig. 9.

In Fig. 9(a) we show the value of $\delta(g-2)_\mu$ versus the dark matter mass in the case where the scalar and pseudoscalar are close to being degenerate, $|m_s - m_a| \lesssim \text{a few GeV}$. The parameter of greatest impact on the $(g-2)_\mu$ calculation is in this case the sum of the new Yukawa couplings, or $c_R^{(s)}$. We show in the figure the dependence of $\delta(g-2)_\mu$ on selected values of $c_R^{(s)}$, when $m_{\tilde{E}} \approx 100 \text{ GeV}$ to avoid LHC bounds, and $|c_R^{(a)}|$ is set to 1. One can see that, as $m_s \approx m_a$ approaches $m_{\tilde{E}}$, the bulk becomes more and more efficient [45] until Ωh^2 drops below the lower bound when $m_{\text{DM}} \approx 80 \text{ GeV}$. At that point, in order to maintain the constraint from $\Omega h^2 \approx 0.12$ in place, the scalar masses must become more separated. Note also that for $m_{\tilde{E}} \approx 100 \text{ GeV}$, a dark matter mass below $\sim 40 \text{ GeV}$ is excluded by the ATLAS 2-lepton search, independently of the value of $c_R^{(s)}$.

In Fig. 9(b) we show the case $m_{\text{DM}} = m_a \ll m_s$. We impose in the plot $m_{\tilde{E}} \approx m_a + 50 \text{ GeV}$, as under this condition one can evade the LHC constraints. Here the scalar particle s effectively decouples from the $(g-2)_\mu$ calculation, thus reproducing the limit of Model 1, with the difference that the coupling of the scalar a to the muon is expressed in terms of

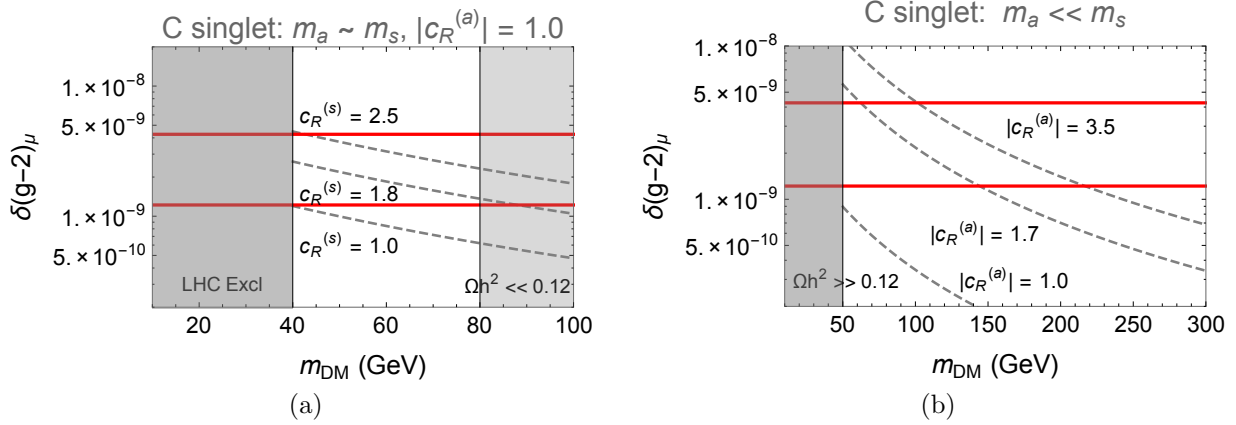


Figure 9: The computed $\delta(g-2)_\mu$ versus the dark matter mass for the parameter space allowed by dark matter in Model 1a (complex singlet scalar and singlet VL fermions). (a) The case of scalar masses being close to degenerate, $m_{\text{DM}} \equiv m_a \approx m_s$, as a function of the coupling to the muon, $c_R^{(s)} = (Y_S + Y_{S^*})/\sqrt{2}$. The new fermion mass is fixed slightly above 100 GeV, and we set the pseudoscalar coupling to $|c_R^{(a)}| = |Y_S - Y_{S^*}|/\sqrt{2} = 1$. The dark matter becomes under-abundant for $m_{\text{DM}} \gtrsim 80$ GeV. (b) The case $m_s \gg m_a$, for different values of the coupling of a to the muon, $|c_R^{(a)}|$. This case resembles the behavior of Model 1.

$$|c_R^{(a)}| = |Y_S - Y_{S^*}|/\sqrt{2}.$$

Similarly to the equivalent cases in Sec. 5.1, if we consider **Model 2a**, in which the complex scalar couples to a doublet VL fermion, the differences with Model 1a are not substantial. However, because of the enlarged production cross section for doublet fermions, the LHC excludes in this case the region shown on the top right in Fig. 8(b), characterized by charged leptons between 400 and 500 GeV.

Model 3a, finally, presents a pattern in the $[m_{\text{DM}}, \Re(c_L^{(s,a)} c_R^{(s,a)*})^{1/2}]$ plane similar to the one depicted in Fig. 7(a), with large regions of the parameter space allowed by the constraints before the bounds from precision and the LHC are applied. With respect to Model 3, however, it appears that in Model 3a the parameter space cannot be easily constrained, because of the larger number of free parameters. In fact, the (m_{E_1}, m_{DM}) -plane plot equivalent to Fig. 7(b) is not very informative in Model 3a, with no clear correlation emerging in the masses of the surviving points. For this reason we do not show this figure here, and we are forced to conclude that a complex scalar singlet with mixing doublet/singlet VL fermion can accommodate Ωh^2 and the $(g-2)_\mu$ anomaly for large ranges of parameters that will possibly avoid most future constraints, as long as the singlet-doublet mixing is not very large.

5.4 Doublet scalar with singlet, doublet, or triplet VL fermions

In order to analyze the doublet scalar case, let us first briefly recall its dark matter properties. Inert doublet scalar dark matter has been analyzed in the literature in several papers (we refer to, e.g., [84,85] for recent studies). When the relic density is driven by the Higgs portal couplings the characteristics are well known. There are two viable regions for dark matter in the parameter space. One for $m_{\text{DM}} \lesssim 100$ GeV and the other in the range from ~ 700 GeV

to several TeV. For the parameter space in between, the dark matter is under-abundant, as at about 85 GeV the annihilation channel $ss(a) \rightarrow W^+W^-$ opens up (in a fashion similar to the higgsino case in supersymmetry). For the models with no fermion mixing, the TeV-range region does not admit solutions for the $(g-2)_\mu$ anomaly, so that we will limit our analysis to scalar masses below ~ 100 GeV.

In Fig. 10(a) we present the now familiar plane of the Yukawa coupling to muons versus the dark matter mass in **Model 4**, which features a doublet scalar and singlet VL fermions in the spectrum. As before, at this stage of the analysis we have not applied the bounds from EWPOs and the LHC. The dark matter in the low-mass region is obtained mostly through the bulk, as values of the portal couplings that might produce $\Omega h^2 \approx 0.12$ through interactions with the Higgs have long been excluded in direct detection experiments (with the exception of the Higgs resonance).

As in the previous cases the $(g-2)_\mu$ anomaly can be fitted in the bulk. Unlike in the complex singlet case, however, solutions with dark matter much lighter than 40 GeV cannot be found here, as LEP has excluded weakly-coupled charged particles below ~ 100 GeV and all scalars belong to the same doublet. Close inspection of Eq. (30) reveals that, once the charged scalar satisfies that constraint, also the pseudoscalar becomes heavier than 100 GeV (recall that $\lambda_3 + \lambda_4 + 2\lambda_5 \ll 1$) and the dark matter sector approaches the limit of Model 1.

A similar plot for **Model 5**, which features a doublet scalar and doublet VL fermions, is shown in Fig. 10(b). After a quick look at Eq. (34) one can see that in this case there is a coupling of the muon to the charged scalar/neutral fermion loop. Thus, we expect $(g-2)_\mu$ to be generally smaller than in Model 4 in the equivalent parameter range, as there is a negative contribution damping its value. Note, in this regard, that the Higgs-resonance region does not present solutions to the $(g-2)_\mu$ anomaly in Model 5 since, in order to avoid excessively diluting Ωh^2 , either the Yukawa couplings should be there quite small, or the VL fermion mass larger than in other regions of the parameter space.

On the other hand, in **Model 7**, characterized by a doublet scalar and triplet VL fermions, simultaneous solutions to the $(g-2)_\mu$ anomaly and dark matter exist *only* in the Higgs-resonance region. In fact, in general, due to the impact of the large doubly-charged contribution, one obtains $\delta(g-2)_\mu$ in the 2σ region for fermion masses that must be quite large, $m_{\Psi^\pm}, m_{\Psi^{\pm\pm}} \gg 100$ GeV. As a consequence, the bulk annihilation cross section is not large enough to yield $\Omega h^2 \approx 0.12$. However, in the Higgs-resonance region, the relic abundance is obtained via portal couplings, so that a solution that can accommodate the $(g-2)_\mu$ anomaly can be easily found for a wide range of Yukawa couplings and fermion mass values.

Finally, we illustrate the case of **Model 8**, characterized by a doublet scalar and adjoint triplet VL fermions, in Fig. 10(d). As one can see from the plot, there is no parameter space here that can accommodate the measured value of $(g-2)_\mu$ and the relic density at the same time. As a matter of fact, in Model 8 the bulk annihilation channel $ss(a) \rightarrow \nu_\mu \nu_\mu$ is so efficient that it effectively places an upper bound on the new Yukawa coupling, $Y_A \lesssim 0.8 - 1$. As a consequence, $\delta(g-2)_\mu$ is never large enough in the region with $\Omega h^2 \approx 0.12$.

The impact of LHC 13 TeV and electroweak precision constraints on the parameter space in agreement with dark matter and the $(g-2)_\mu$ anomaly for Models 4-8 is shown in Fig. 11. In all scenarios, as long as the charged fermion is situated around 100 GeV a compressed region can be observed, which survives all of the constraints. Outside of the compressed region, across the Higgs resonance the mass of the charged VL fermions becomes larger to

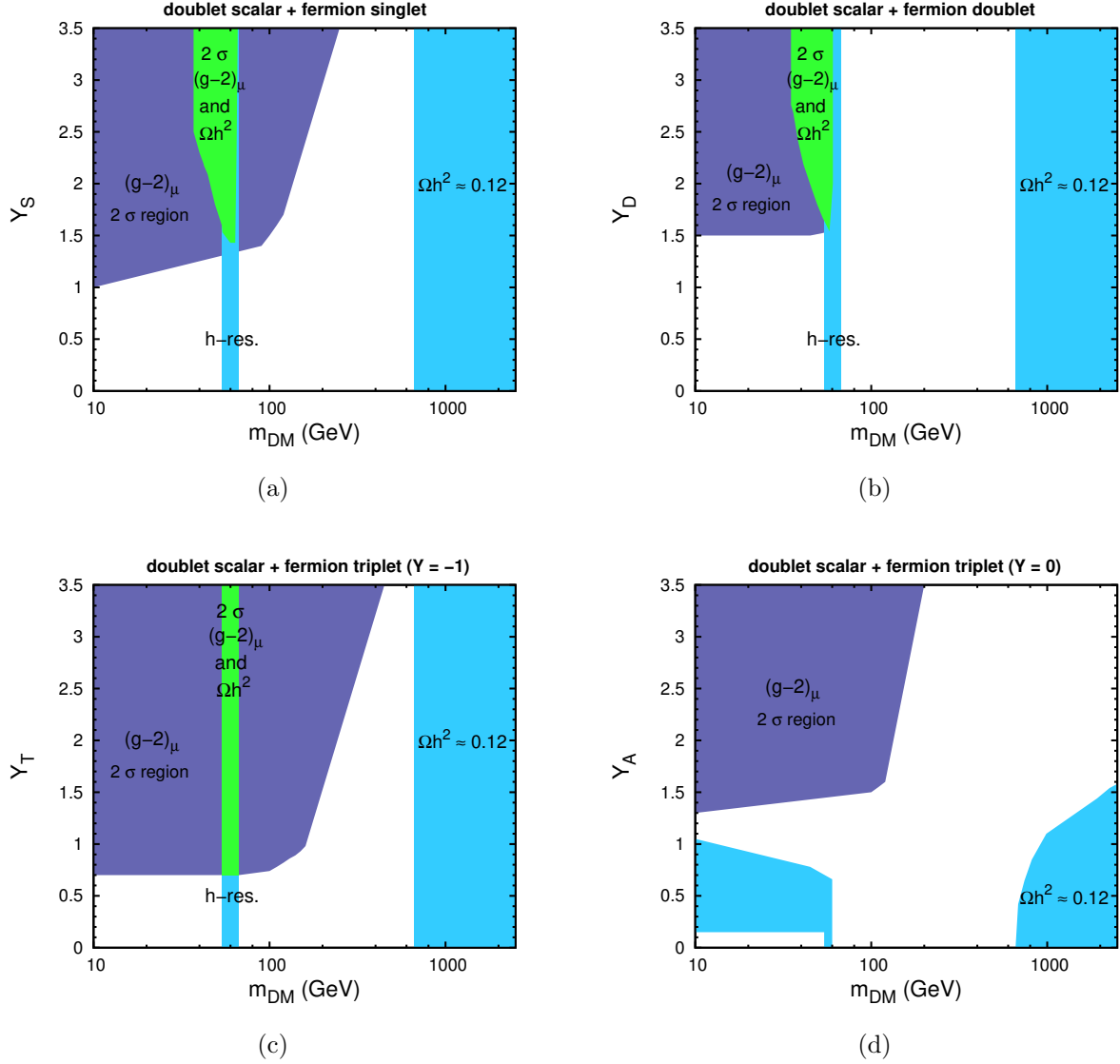


Figure 10: Planes of the Yukawa coupling to muons versus the dark matter mass in models with a scalar doublet. The region where the $(g-2)_\mu$ anomaly can be accommodated at 2σ is shown in blue, the region where the relic abundance is correct within 2σ is shown in cyan, and the combined parameter space is highlighted in green. (a) Model 4 (doublet scalar and singlet VL fermions), (b) Model 5 (doublet scalar and doublet VL fermions), (c) Model 7 (doublet scalar and triplet VL fermions), (d) Model 8 (doublet scalar and adjoint triplet VL fermions).

suppress bulk annihilation. In Model 4 the LHC 2-lepton search places a lower bound on the fermions mass of about 160 GeV. It is much weaker than the corresponding bound for Model 1, as in Model 4 the decay $E' \rightarrow S^+ \bar{\nu}_\mu$ is possible, which cuts drastically the efficiency of the search due to a reduced branching ratio to the 2-lepton signal.

As before, we have also calculated the effect of the future LHC reach with 300 fb^{-1} on

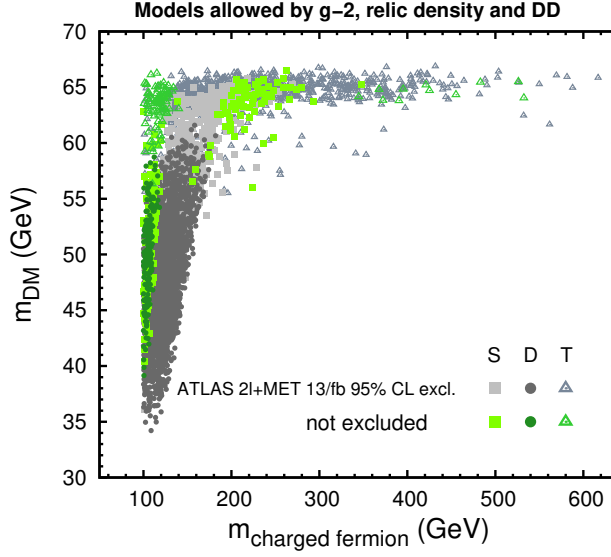


Figure 11: The impact of LHC 13 TeV on the parameter space in agreement with dark matter and the $(g - 2)_\mu$ anomaly in Models 4 (squares), 5 (circles), and 7 (triangles). The points allowed are shown in three different shades of green, while those excluded in three different shades of gray.

the models. Most of the currently allowed regions with fermion mass larger than ~ 100 GeV will be strongly reduced at the end of the current LHC run, although it does not appear that any of them can be probed in its absolute entirety even with large luminosity.

We summarize the findings of this subsection in Fig. 12, where we present the value of $\delta(g - 2)_\mu$ versus the scalar dark matter mass in every model for a fixed value of the new Yukawa coupling $Y = 2$. The only exception is Model 8 for which, as we saw in Fig. 10(d), there exist an upper bound on the Yukawa coupling due to the relic abundance. To avoid the bounds from the LHC, in Fig. 12 we have set the charged fermion mass just above 100 GeV, while the pseudoscalar and charged scalar mass are fixed case by case to the typical values observed in the scans. As the mass of the scalar s approaches the Higgs resonance, however, we move the fermion mass up to larger values, to mimic the behavior of the scans. As a consequence, $\delta(g - 2)_\mu$ drops.

Note that in Model 5 (magenta dashed) $Y_D \approx 2$ barely allows the model to sit inside the 2σ region for $(g - 2)_\mu$. As we discussed above, since in the Higgs-resonance either the allowed Yukawa coupling for $\Omega h^2 \approx 0.12$ is much smaller than 2, or the fermion mass must be larger than 100 GeV, it follows that in the Higgs-resonance there is no common parameter space for $(g - 2)_\mu$ and dark matter. Conversely in Model 7 (blue dot-dashed), for $Y_T \approx 2$ the model sits generally above the 2σ region for $(g - 2)_\mu$. Only the significant drop in the Yukawa coupling necessary to get $\Omega h^2 \approx 0.12$ in the Higgs resonance can bring its value back into the allowed region.

We finally comment on the numerical results we get for **Model 9**, characterized by the mixing of the adjoint triplet fermions and the doublet fermions. As we mentioned when we introduced Eq. (42), several substantial contributions to $(g - 2)_\mu$ arise in this model, as the

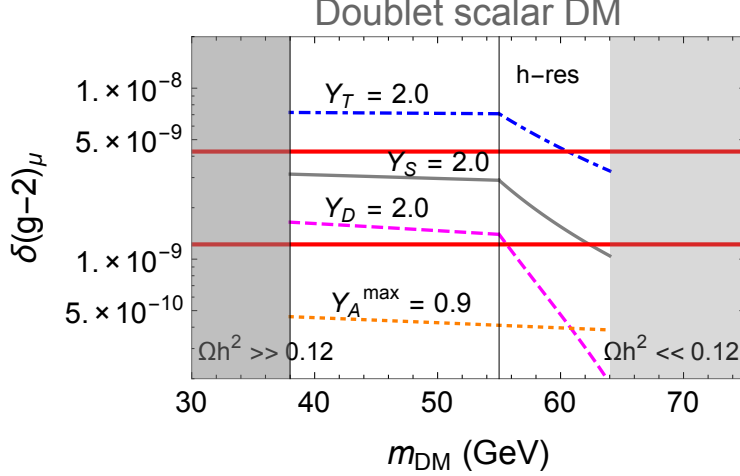


Figure 12: The computed $\delta(g-2)_\mu$ as a function of the dark matter mass $m_{\text{DM}} = m_s$ and Yukawa coupling to the muon in the models with a doublet scalar, discussed in Sec. 5.4. The charged fermion mass is fixed at about 100 GeV outside of the Higgs resonance to evade the LHC bounds, but it is progressively pushed to larger values on the resonance region. The pseudoscalar and charged scalar mass are fixed case by case to the typical values observed in the scans. Gray solid line: singlet VL fermions; magenta dashed line: doublet VL fermions; blue dot-dashed line: triplet VL fermions; orange dotted line: adjoint triplet VL fermions.

neutral scalar/charged fermion and pseudoscalar/charged fermion contributions sum up, and one also has the positive contribution from the mixing heavy neutrinos and charged scalar. As a consequence, solutions to the $(g-2)_\mu$ anomaly can be potentially found in the large dark-matter mass region, $m_{\text{DM}} \gtrsim 800$ GeV. However, since the Yukawa coupling is always quite limited in size, the solutions we found in our scans are all characterized by large mixing angles, and inevitably fail to pass the constraints from EWPOs. Thus, up to the possibility of having missed some fine-tuned corners of the parameter space, we conclude that there is no solution for $(g-2)_\mu$ and dark matter in Model 9.

6 Summary and conclusions

In this paper we have drawn some predictions for future measurements of $(g-2)_\mu$ under the hypothesis that the anomaly measured at BNL will be confirmed and that the same underlying BSM physics is responsible for the relic abundance of dark matter in the Universe.

To investigate these scenarios, we have constructed a set of renormalizable, $\text{SU}(2) \times \text{U}(1)$ invariant extensions of the SM, each comprising inert \mathbb{Z}_2 -odd scalar fields and one or more VL pair of colorless fermions that communicate to the SM muons through Yukawa-type interactions. Our new sectors are classified according to their transformation properties under the SM gauge group: real singlet, complex singlet, and doublet scalars, with all possible types of VL fermions allowed by the gauge symmetry. All models have been systematically confronted with a variety of experimental constraints: LEP mass bounds, direct LHC searches, electroweak precision observables, and direct searches for dark matter.

In general, the presence of a muon portal introduces a well known t -channel bulk mechanism for the dark matter relic density that extends the widely studied Higgs portal and allows one to evade strong bounds from direct detection experiments. In the case of a real singlet scalar dark matter particle, we find that before applying the LHC bounds both relic density and $\delta(g-2)_\mu$ can be accommodated for $m_{\text{DM}} \approx 40 - 160 \text{ GeV}$, provided VL fermions are lighter than 350 GeV and the Yukawa coupling exceeds ~ 1.2 . The same pattern is observed for singlet and doublet fermions, since in both cases only the charged component contributes to the anomalous magnetic moment of the muon. When LHC bounds are applied, the parameter space is in large part excluded by the ATLAS 2-lepton + missing E_T search, except the region where the mass difference between the dark matter scalar and fermion drops below $\sim 70 \text{ GeV}$. Interestingly, future high-precision experiments like GigaZ and TLEP have the potential to probe this region entirely, as the new sector generates small but non-zero corrections to the $Z\mu\bar{\mu}$ vertex.

If the singlet scalar is complex, the region where $(g-2)_\mu$ and relic density are satisfied extends down to around 10 GeV before the LHC bounds are applied, as additional annihilation channels are open due to the presence of a pseudoscalar particle in the spectrum. The lower bound on the allowed Yukawa coupling is reduced to ~ 0.5 , since there are two Yukawa couplings summing up. For the same reason, fermions up to $\sim 500 \text{ GeV}$ are allowed since there are two contributions to $(g-2)_\mu$.

For both the real and complex singlet scalar, we have additionally allowed the singlet and doublet VL fermions to mix through interactions with the SM Higgs, thus introducing a source of chiral-symmetry violation that, by being proportional to the mass of the heavy leptons, can boost $\delta(g-2)_\mu$. The anomaly can thus be accommodated for masses up to $\sim 3 \text{ TeV}$. The same effect, however, generates large contributions to the EWPOs that, for the large fermion mixing, exclude part of the parameter space. In particular, we find that in the real scalar case with mixing VL fermions the viable part of the parameter space can be probed almost entirely by a combination of the LHC, dark matter direct detection, and future electroweak precision experiments.

The parameter space is more constrained by the relic density in cases with an $\text{SU}(2)$ scalar doublet. Typical masses range from $m_{\text{DM}} \approx 40 \text{ GeV}$ to the Higgs-resonance, $m_{\text{DM}} \approx m_h/2$. Most of the parameter space is almost entirely tested by LHC 2-lepton searches, except the region of compressed spectra, when the new fermions and scalars are almost degenerate. Interesting properties arise particularly in the case with $\text{SU}(2)$ triplet fermions, thanks to the well known presence of a doubly charged lepton in the spectrum, which can enhance the calculation of $\delta(g-2)_\mu$.

Overall, our study shows that scenarios with one type of BSM scalar and fermions, which in general can accommodate $(g-2)_\mu$ for a relatively large range of masses and Yukawa couplings, become strongly constrained when the relic density is added to the set of assumptions. That makes them very predictive in case a positive measurement is confirmed at Fermilab or J-PARC. That is in general not true, however, for scenarios with singlet-doublet mixing, since the number of free parameters is large enough to accommodate both $(g-2)_\mu$ and Ωh^2 and evade other experimental constraints. For these scenarios, increased precision measurements of Z -physics observables in future electron-positron colliders will be able to disentangle some of the degeneracies.

ACKNOWLEDGMENTS

We would like to thank Luc Darmé for valuable input on the interface of **SARAH** with **MultiNest**, Florian Staub for helpful correspondence regarding **SARAH**, Joachim Brod and Wei-Chih Huang for discussions. KK is supported in part by the DFG Research Unit FOR 1873 “Quark Flavour Physics and Effective Field Theories”. The work of EMS is supported by the Alexander von Humboldt Foundation. The use of the CIS computer cluster at the National Centre for Nuclear Research in Warsaw is gratefully acknowledged.

References

- [1] **Muon g-2** Collaboration, G. W. Bennett *et al.*, “Final Report of the Muon E821 Anomalous Magnetic Moment Measurement at BNL,” *Phys. Rev.* **D73** (2006) 072003, [arXiv:hep-ex/0602035](#) [[hep-ex](#)].
- [2] M. Davier, “Update of the Hadronic Vacuum Polarisation Contribution to the muon g-2,” in *14th International Workshop on Tau Lepton Physics (TAU 2016) Beijing, China, September 19-23, 2016*. 2016. [arXiv:1612.02743](#) [[hep-ph](#)]. <https://inspirehep.net/record/1502365/files/arXiv:1612.02743.pdf>.
- [3] F. Jegerlehner, “Muon g-2 Theory: the Hadronic Part,” [arXiv:1705.00263](#) [[hep-ph](#)].
- [4] **Muon g-2** Collaboration, J. Grange *et al.*, “Muon (g-2) Technical Design Report,” [arXiv:1501.06858](#) [[physics.ins-det](#)].
- [5] **Muon g-2** Collaboration, A. Chapelain, “The Muon g-2 experiment at Fermilab,” *EPJ Web Conf.* **137** (2017) 08001, [arXiv:1701.02807](#) [[physics.ins-det](#)].
- [6] **Muon g-2** Collaboration, K. Ishida, “Ultra slow muon source for new muon g-2 experiment,” *AIP Conf. Proc.* **1222** (2010) 396–399.
- [7] **J-PARC g-2** Collaboration, T. Mibe, “New g-2 experiment at J-PARC,” *Chin. Phys.* **C34** (2010) 745–748.
- [8] **J-PARC muon g-2/EDM** Collaboration, H. Inuma, “New approach to the muon g-2 and EDM experiment at J-PARC,” *J. Phys. Conf. Ser.* **295** (2011) 012032.
- [9] **J-PARC g-’2/EDM** Collaboration, N. Saito, “A novel precision measurement of muon g-2 and EDM at J-PARC,” *AIP Conf. Proc.* **1467** (2012) 45–56.
- [10] **E34** Collaboration, M. Otani, “Status of the Muon g-2/EDM Experiment at J-PARC (E34),” *JPS Conf. Proc.* **8** (2015) 025008.
- [11] F. Jegerlehner and A. Nyffeler, “The Muon g-2,” *Phys. Rept.* **477** (2009) 1–110, [arXiv:0902.3360](#) [[hep-ph](#)].
- [12] J. P. Leveille, “The Second Order Weak Correction to (G-2) of the Muon in Arbitrary Gauge Models,” *Nucl. Phys.* **B137** (1978) 63–76.

- [13] S. R. Moore, K. Whisnant, and B.-L. Young, “Second Order Corrections to the Muon Anomalous Magnetic Moment in Alternative Electroweak Models,” *Phys. Rev.* **D31** (1985) 105.
- [14] P. Fayet, in *Unification of the Fundamental Particle Interactions*, edited by S. Ferrara, J. Ellis, and P. van Nieuwenhuizen (Plenum, New York, 1980), p. 587.
- [15] J. A. Grifols and A. Mendez, “Constraints on Supersymmetric Particle Masses From $(g - 2) \mu$,” *Phys. Rev.* **D26** (1982) 1809.
- [16] J. R. Ellis, J. S. Hagelin, and D. V. Nanopoulos, “Spin 0 Leptons and the Anomalous Magnetic Moment of the Muon,” *Phys. Lett.* **B116** (1982) 283–286.
- [17] R. Barbieri and L. Maiani, “The Muon Anomalous Magnetic Moment in Broken Supersymmetric Theories,” *Phys. Lett.* **B117** (1982) 203–207.
- [18] J. C. Romao, A. Barroso, M. C. Bento, and G. C. Branco, “Flavor Violation in Supersymmetric Theories,” *Nucl. Phys.* **B250** (1985) 295–311.
- [19] D. A. Kosower, L. M. Krauss, and N. Sakai, “Low-Energy Supergravity and the Anomalous Magnetic Moment of the Muon,” *Phys. Lett.* **B133** (1983) 305–310.
- [20] T. C. Yuan, R. L. Arnowitt, A. H. Chamseddine, and P. Nath, “Supersymmetric Electroweak Effects on $G-2 (\mu)$,” *Z. Phys.* **C26** (1984) 407.
- [21] I. Vendramin, “Constraints on Supersymmetric Parameters from Muon Magnetic Moment,” *Nuovo Cim.* **A101** (1989) 731.
- [22] T. Moroi, “The Muon anomalous magnetic dipole moment in the minimal supersymmetric standard model,” *Phys. Rev.* **D53** (1996) 6565–6575, [arXiv:hep-ph/9512396 \[hep-ph\]](#). [Erratum: *Phys. Rev.* **D56**, 4424 (1997)].
- [23] G.-C. Cho, K. Hagiwara, and M. Hayakawa, “Muon $g-2$ and precision electroweak physics in the MSSM,” *Phys. Lett.* **B478** (2000) 231–238, [arXiv:hep-ph/0001229 \[hep-ph\]](#).
- [24] S. P. Martin and J. D. Wells, “Muon anomalous magnetic dipole moment in supersymmetric theories,” *Phys. Rev.* **D64** (2001) 035003, [arXiv:hep-ph/0103067 \[hep-ph\]](#).
- [25] A. Czarnecki and W. J. Marciano, “The Muon anomalous magnetic moment: A Harbinger for ‘new physics’,” *Phys. Rev.* **D64** (2001) 013014, [arXiv:hep-ph/0102122 \[hep-ph\]](#).
- [26] K. R. Lynch, “A Note on one loop electroweak contributions to $g-2$: A Companion to BUHEP-01-16,” [arXiv:hep-ph/0108081 \[hep-ph\]](#).
- [27] A. Freitas, J. Lykken, S. Kell, and S. Westhoff, “Testing the Muon $g-2$ Anomaly at the LHC,” *JHEP* **05** (2014) 145, [arXiv:1402.7065 \[hep-ph\]](#). [Erratum: *JHEP* **09**, 155 (2014)].

- [28] F. S. Queiroz and W. Shepherd, “New Physics Contributions to the Muon Anomalous Magnetic Moment: A Numerical Code,” *Phys. Rev.* **D89** no. 9, (2014) 095024, [arXiv:1403.2309 \[hep-ph\]](#).
- [29] M. Lindner, M. Platscher, and F. S. Queiroz, “A Call for New Physics : The Muon Anomalous Magnetic Moment and Lepton Flavor Violation,” [arXiv:1610.06587 \[hep-ph\]](#).
- [30] G. Belanger, C. Delaunay, and S. Westhoff, “A Dark Matter Relic From Muon Anomalies,” *Phys. Rev.* **D92** (2015) 055021, [arXiv:1507.06660 \[hep-ph\]](#).
- [31] P. Agrawal, Z. Chacko, and C. B. Verhaaren, “Leptophilic Dark Matter and the Anomalous Magnetic Moment of the Muon,” *JHEP* **08** (2014) 147, [arXiv:1402.7369 \[hep-ph\]](#).
- [32] **LHCb** Collaboration, R. Aaij *et al.*, “Test of lepton universality with $B^0 \rightarrow K^{*0} \ell^+ \ell^-$ decays,” [arXiv:1705.05802 \[hep-ex\]](#).
- [33] K. Kannike, M. Raidal, D. M. Straub, and A. Strumia, “Anthropic solution to the magnetic muon anomaly: the charged see-saw,” *JHEP* **02** (2012) 106, [arXiv:1111.2551 \[hep-ph\]](#). [Erratum: *JHEP*10,136(2012)].
- [34] S. Kanemitsu and K. Tobe, “New physics for muon anomalous magnetic moment and its electroweak precision analysis,” *Phys. Rev.* **D86** (2012) 095025, [arXiv:1207.1313 \[hep-ph\]](#).
- [35] R. Dermisek and A. Raval, “Explanation of the Muon g-2 Anomaly with Vector-like Leptons and its Implications for Higgs Decays,” *Phys. Rev.* **D88** (2013) 013017, [arXiv:1305.3522 \[hep-ph\]](#).
- [36] J. McDonald, “Gauge singlet scalars as cold dark matter,” *Phys. Rev.* **D50** (1994) 3637–3649, [arXiv:hep-ph/0702143 \[HEP-PH\]](#).
- [37] M. C. Bento, O. Bertolami, R. Rosenfeld, and L. Teodoro, “Selfinteracting dark matter and invisibly decaying Higgs,” *Phys. Rev.* **D62** (2000) 041302, [arXiv:astro-ph/0003350 \[astro-ph\]](#).
- [38] C. P. Burgess, M. Pospelov, and T. ter Veldhuis, “The Minimal model of non-baryonic dark matter: A Singlet scalar,” *Nucl. Phys.* **B619** (2001) 709–728, [arXiv:hep-ph/0011335 \[hep-ph\]](#).
- [39] H. Davoudiasl, R. Kitano, T. Li, and H. Murayama, “The New minimal standard model,” *Phys. Lett.* **B609** (2005) 117–123, [arXiv:hep-ph/0405097 \[hep-ph\]](#).
- [40] B. Patt and F. Wilczek, “Higgs field portal into hidden sectors,” [arXiv:hep-ph/0605188 \[hep-ph\]](#).
- [41] V. Barger, P. Langacker, M. McCaskey, M. J. Ramsey-Musolf, and G. Shaughnessy, “LHC Phenomenology of an Extended Standard Model with a Real Scalar Singlet,” *Phys. Rev.* **D77** (2008) 035005, [arXiv:0706.4311 \[hep-ph\]](#).

- [42] **XENON** Collaboration, E. Aprile *et al.*, “First Dark Matter Search Results from the XENON1T Experiment,” [arXiv:1705.06655](#) [[astro-ph.CO](#)].
- [43] M. Drees and M. M. Nojiri, “The Neutralino relic density in minimal $N = 1$ supergravity,” *Phys. Rev.* **D47** (1993) 376–408, [arXiv:hep-ph/9207234](#) [[hep-ph](#)].
- [44] H. Baer and M. Brhlik, “Cosmological relic density from minimal supergravity with implications for collider physics,” *Phys. Rev.* **D53** (1996) 597–605, [arXiv:hep-ph/9508321](#) [[hep-ph](#)].
- [45] Y. Bai and J. Berger, “Lepton Portal Dark Matter,” *JHEP* **08** (2014) 153, [arXiv:1402.6696](#) [[hep-ph](#)].
- [46] K. Fukushima, C. Kelso, J. Kumar, P. Sandick, and T. Yamamoto, “MSSM dark matter and a light slepton sector: The incredible bulk,” *Phys. Rev.* **D90** no. 9, (2014) 095007, [arXiv:1406.4903](#) [[hep-ph](#)].
- [47] **ATLAS** Collaboration, “Search for supersymmetry with two and three leptons and missing transverse momentum in the final state at 13 TeV with the ATLAS detector,”.
- [48] **ATLAS** Collaboration, M. Aaboud *et al.*, “Search for new phenomena in final states with an energetic jet and large missing transverse momentum in pp collisions at 13 TeV using the ATLAS detector,” *Phys. Rev.* **D94** no. 3, (2016) 032005, [arXiv:1604.07773](#) [[hep-ex](#)].
- [49] **Particle Data Group** Collaboration, C. Patrignani *et al.*, “Review of Particle Physics,” *Chin. Phys.* **C40** no. 10, (2016) 100001.
- [50] D. S. Akerib *et al.*, “Results from a search for dark matter in the complete LUX exposure,” [arXiv:1608.07648](#) [[astro-ph.CO](#)].
- [51] V. Barger, P. Langacker, M. McCaskey, M. Ramsey-Musolf, and G. Shaughnessy, “Complex Singlet Extension of the Standard Model,” *Phys. Rev.* **D79** (2009) 015018, [arXiv:0811.0393](#) [[hep-ph](#)].
- [52] M. Gonderinger, H. Lim, and M. J. Ramsey-Musolf, “Complex Scalar Singlet Dark Matter: Vacuum Stability and Phenomenology,” *Phys. Rev.* **D86** (2012) 043511, [arXiv:1202.1316](#) [[hep-ph](#)].
- [53] R. Barbieri, L. J. Hall, and V. S. Rychkov, “Improved naturalness with a heavy Higgs: An Alternative road to LHC physics,” *Phys. Rev.* **D74** (2006) 015007, [arXiv:hep-ph/0603188](#) [[hep-ph](#)].
- [54] E. Ma, “Verifiable radiative seesaw mechanism of neutrino mass and dark matter,” *Phys. Rev.* **D73** (2006) 077301, [arXiv:hep-ph/0601225](#) [[hep-ph](#)].
- [55] E. Ma, “Common origin of neutrino mass, dark matter, and baryogenesis,” *Mod. Phys. Lett.* **A21** (2006) 1777–1782, [arXiv:hep-ph/0605180](#) [[hep-ph](#)].

- [56] L. Lopez Honorez, E. Nezri, J. F. Oliver, and M. H. G. Tytgat, “The Inert Doublet Model: An Archetype for Dark Matter,” *JCAP* **0702** (2007) 028, [arXiv:hep-ph/0612275](#) [hep-ph].
- [57] D. Majumdar and A. Ghosal, “Dark Matter candidate in a Heavy Higgs Model - Direct Detection Rates,” *Mod. Phys. Lett. A* **23** (2008) 2011–2022, [arXiv:hep-ph/0607067](#) [hep-ph].
- [58] T. Araki, C. Q. Geng, and K. I. Nagao, “Dark Matter in Inert Triplet Models,” *Phys. Rev. D* **83** (2011) 075014, [arXiv:1102.4906](#) [hep-ph].
- [59] **SLD Electroweak Group, DELPHI, ALEPH, SLD, SLD Heavy Flavour Group, OPAL, LEP Electroweak Working Group, L3 Collaboration**, S. Schael *et al.*, “Precision electroweak measurements on the Z resonance,” *Phys. Rept.* **427** (2006) 257–454, [arXiv:hep-ex/0509008](#) [hep-ex].
- [60] K. Hagiwara, S. Matsumoto, D. Haidt, and C. S. Kim, “A Novel approach to confront electroweak data and theory,” *Z. Phys.* **C64** (1994) 559–620, [arXiv:hep-ph/9409380](#) [hep-ph]. [Erratum: *Z. Phys.* **C68**, 352(1995)].
- [61] G.-C. Cho and K. Hagiwara, “Supersymmetry versus precision experiments revisited,” *Nucl. Phys. B* **574** (2000) 623–674, [arXiv:hep-ph/9912260](#) [hep-ph].
- [62] T. Hahn and M. Perez-Victoria, “Automatized one loop calculations in four-dimensions and D-dimensions,” *Comput. Phys. Commun.* **118** (1999) 153–165, [arXiv:hep-ph/9807565](#) [hep-ph].
- [63] M. E. Peskin and T. Takeuchi, “Estimation of oblique electroweak corrections,” *Phys. Rev. D* **46** (1992) 381–409.
- [64] A. Joglekar, P. Schwaller, and C. E. M. Wagner, “Dark Matter and Enhanced Higgs to Di-photon Rate from Vector-like Leptons,” *JHEP* **12** (2012) 064, [arXiv:1207.4235](#) [hep-ph].
- [65] J. Erler, S. Heinemeyer, W. Hollik, G. Weiglein, and P. M. Zerwas, “Physics impact of GigaZ,” *Phys. Lett. B* **486** (2000) 125–133, [arXiv:hep-ph/0005024](#) [hep-ph]. [1389(2000)].
- [66] H. Baer, T. Barklow, K. Fujii, Y. Gao, A. Hoang, S. Kanemura, J. List, H. E. Logan, A. Nomerotski, M. Perelstein, *et al.*, “The International Linear Collider Technical Design Report - Volume 2: Physics,” [arXiv:1306.6352](#) [hep-ph].
- [67] **TLEP Design Study Working Group** Collaboration, M. Bicer *et al.*, “First Look at the Physics Case of TLEP,” *JHEP* **01** (2014) 164, [arXiv:1308.6176](#) [hep-ex].
- [68] K. Kowalska, L. Roszkowski, E. M. Sessolo, and A. J. Williams, “GUT-inspired SUSY and the muon $g-2$ anomaly: prospects for LHC 14 TeV,” *JHEP* **06** (2015) 020, [arXiv:1503.08219](#) [hep-ph].

- [69] K. Kowalska, “Phenomenological MSSM in light of new 13 TeV LHC data,” *Eur. Phys. J.* **C76** no. 12, (2016) 684, [arXiv:1608.02489 \[hep-ph\]](#).
- [70] **CMS Collaboration**, C. Collaboration, “Searches for invisible Higgs boson decays with the CMS detector,”.
- [71] **Planck Collaboration**, P. A. R. Ade *et al.*, “Planck 2015 results. XIII. Cosmological parameters,” *Astron. Astrophys.* **594** (2016) A13, [arXiv:1502.01589 \[astro-ph.CO\]](#).
- [72] F. Staub, “SARAH 4 : A tool for (not only SUSY) model builders,” *Comput. Phys. Commun.* **185** (2014) 1773–1790, [arXiv:1309.7223 \[hep-ph\]](#).
- [73] W. Porod, “SPheno, a program for calculating supersymmetric spectra, SUSY particle decays and SUSY particle production at e+ e- colliders,” *Comput. Phys. Commun.* **153** (2003) 275–315, [arXiv:hep-ph/0301101 \[hep-ph\]](#).
- [74] W. Porod and F. Staub, “SPheno 3.1: Extensions including flavour, CP-phases and models beyond the MSSM,” *Comput. Phys. Commun.* **183** (2012) 2458–2469, [arXiv:1104.1573 \[hep-ph\]](#).
- [75] W. Porod, F. Staub, and A. Vicente, “A Flavor Kit for BSM models,” *Eur. Phys. J.* **C74** no. 8, (2014) 2992, [arXiv:1405.1434 \[hep-ph\]](#).
- [76] A. Belyaev, N. D. Christensen, and A. Pukhov, “CalcHEP 3.4 for collider physics within and beyond the Standard Model,” *Comput. Phys. Commun.* **184** (2013) 1729–1769, [arXiv:1207.6082 \[hep-ph\]](#).
- [77] G. Belanger, F. Boudjema, A. Pukhov, and A. Semenov, “micrOMEGAs 3: A program for calculating dark matter observables,” *Comput. Phys. Commun.* **185** (2014) 960–985, [arXiv:1305.0237 \[hep-ph\]](#).
- [78] F. Feroz, M. Hobson, and M. Bridges, “MultiNest: an efficient and robust Bayesian inference tool for cosmology and particle physics,” *Mon. Not. Roy. Astron. Soc.* **398** (2009) 1601–1614, [arXiv:0809.3437 \[astro-ph\]](#).
- [79] J. Alwall, R. Frederix, S. Frixione, V. Hirschi, F. Maltoni, O. Mattelaer, H. S. Shao, T. Stelzer, P. Torrielli, and M. Zaro, “The automated computation of tree-level and next-to-leading order differential cross sections, and their matching to parton shower simulations,” *JHEP* **07** (2014) 079, [arXiv:1405.0301 \[hep-ph\]](#).
- [80] T. Sjostrand, S. Mrenna, and P. Z. Skands, “A Brief Introduction to PYTHIA 8.1,” *Comput. Phys. Commun.* **178** (2008) 852–867, [arXiv:0710.3820 \[hep-ph\]](#).
- [81] **DELPHES 3 Collaboration**, J. de Favereau *et al.*, “DELPHES 3, A modular framework for fast simulation of a generic collider experiment,” *JHEP* **1402** (2014) 057, [arXiv:1307.6346 \[hep-ex\]](#).
- [82] J. Braathen, M. D. Goodsell, and F. Staub, “Supersymmetric and non-supersymmetric models without catastrophic Goldstone bosons,” [arXiv:1706.05372 \[hep-ph\]](#).

- [83] T. Hambye and M. H. G. Tytgat, “Electroweak symmetry breaking induced by dark matter,” *Phys. Lett.* **B659** (2008) 651–655, [arXiv:0707.0633 \[hep-ph\]](#).
- [84] A. Goudelis, B. Herrmann, and O. Stal, “Dark matter in the Inert Doublet Model after the discovery of a Higgs-like boson at the LHC,” *JHEP* **09** (2013) 106, [arXiv:1303.3010 \[hep-ph\]](#).
- [85] A. Arhrib, Y.-L. S. Tsai, Q. Yuan, and T.-C. Yuan, “An Updated Analysis of Inert Higgs Doublet Model in light of the Recent Results from LUX, PLANCK, AMS-02 and LHC,” *JCAP* **1406** (2014) 030, [arXiv:1310.0358 \[hep-ph\]](#).